nagra.

Arbeitsbericht NAB 13-45

Diagnostic analyses of the geomechanical data bases from the SLA-1 borehole

June 2013

V. Favero, A. Ferrari, L. Laloui

Swiss Federal Institute of Technology, Lausanne (EPFL)

Nationale Genossenschaft für die Lagerung radioaktiver Abfälle

Hardstrasse 73
CH-5430 Wettingen
Telefon 056-437 11 11

www.nagra.ch

nagra.

Arbeitsbericht NAB 13-45

Diagnostic analyses of the geomechanical data bases from the SLA-1 borehole

June 2013

V. Favero, A. Ferrari, L. Laloui

Swiss Federal Institute of Technology,
Lausanne (EPFL)

KEYWORDS

Schlattingen SLA-1, Opalinus Clay, geomechanical characterization, rock strength, triaxial tests, UCS, diagnostic analysis

**Nationale Genossenschaft
für die Lagerung
radioaktiver Abfälle**

Hardstrasse 73
CH-5430 Wettingen
Telefon 056-437 11 11

www.nagra.ch

Nagra Working Reports concern work in progress that may have had limited review. They are intended to provide rapid dissemination of information. The viewpoints presented and conclusions reached are those of the author(s) and do not necessarily represent those of Nagra.

Table of Contents

List of Tables

List of Figures

1 Introduction

1.1 Background

The Laboratory for Soil Mechanics (LMS) of the Swiss Federal Institute of Technology in Lausanne (EPFL) together with Gesteinslabor Jahns have been involved in a comprehensive geomechanical testing program on core samples extracted from the deep geothermal well SLA-1 near the village of Schlattingen in the Molasse Basin of Northern Switzerland (Albert et al. 2012). The LMS/EPFL studies emphasized the characterization of the three candidate host rock formations for the disposal of radioactive waste, namely the Effingen Member, the so-called 'Brown Dogger' (stratigraphic sequence of Callovian, Bathonian and Bajocian age) and the Opalinus Clay. Gesteinslabor Jahns concentrated on the Opalinus Clay. The laboratory program comprised geotechnical identification tests, determination of the water retention behaviour and hydro-mechanical tests (oedometer, uniaxial and triaxial tests). The results of the laboratory investigations (Ferrari et al. 2013; Jahns 2013) are feeding in Nagra's geomechanical data base of the potential host rock formations.

In this context LMS/EPFL has been requested to carry out a comprehensive review and interpretation of the relevant geomechanical data base of the Opalinus Clay formation. The interpretation draws on diagnostic analyses of the geomechanical tests on the core samples from Schlattingen and on the identification of the prevailing deformation mechanisms. This includes an assessment of the relevance of the coupled processes (variable saturation and swelling) on the deformation behaviour. Representative values of rock strength and elastic properties of the Opalinus Clay are derived.

The analysis and the evaluation of the findings are carried out in the context of a generalized geomechanical framework for the constitutive behaviour of Opalinus Clay.

1.2 Objectives

This report is aimed at an integrated interpretation of geomechanical laboratory investigations on core samples from the Opalinus Clay formation. The objectives of the data analyses are:

- General quality assessment of the existing geomechanical data bases from SLA-1 and evaluation of the suitability of the data for constitutive modelling of the deformation behaviour of Opalinus Clay.
- Diagnostic analysis of the geomechanical data base from the triaxial testing campaign (Jahns 2013) of the P, S, X and Z samples. The analyses comprise diagnostic plots of the consolidation phase (saturation/consolidation curves) and of the shear phase (p'-q; ε_a-q; ε_a-Δu; ε_a -ε_v).
- Derivation of representative strength and stiffness parameters
- Assessment of the relevance of coupled processes on the deformation behaviour (porosity dependency on retention properties, swelling).
- Further data interpretations in the light of the constitutive modelling of Opalinus Clay.

1.3 Report organization

The report summarizes the results of the diagnostic interpretation of geomechanical laboratory data from the SLA-1 borehole. Scope, objectives and report outline are presented in Chapter 1. Chapter 2 is dedicated to a general review of the existing geomechanical data base. Chapter 3 describes the diagnostic analyses of the geomechanical data base from the triaxial testing campaign. The relevance of coupled processes on the deformation behaviour is assessed in Chapter 4. Further considerations are presented in Chapter 5 in the light of the constitutive modelling of Opalinus Clay. The main achievements are concluded in Chapter 6.

2 Review of the relevant geomechanical databases from SLA-1

The relevant geomechanical data base considered for the analysis of the deformation behaviour of Opalinus Clay comprises a series of geomechanical tests carried out at LMS/EPFL and laboratory tests by the Gesteinslabor Dr. Eberhard Jahns.

The considered tests subjected to diagnostic analysis are the following:

- Material identification tests
- Undrained triaxial tests
- UCS tests
- High pressure oedometer tests
- Swelling tests
- Water retention curves with volume change measurement

A detailed description of the testing devices and methodologies adopted for the performance of the above mentioned tests can be found in Jahns (2013) for what concern the undrained triaxial tests and the UCS tests, and in Ferrari et al. (2013) for what concern the material identification, the high pressure oedometer tests, the swelling tests and the water retention curves. Table 2-1 reports the tests considered in this proposed work, the sample tested together with their ID codes and the sample orientation respect to the bedding planes direction.

Tab. 2-1: Tests from Jahns (2013) considered in the comprehensive analysis and tests IDs.

Test results from NAB13-18 (Jahns 2013)			
Specimen name	Core	Test ID in the report	Orientation to bedding [°]
Triaxial tests			
OPA_VR1_KM69_01	69	KM69_01	90
OPA_VR1_KM69_02	69	KM69_02	90
OPA_VR1_KM69_03	69	KM69_03	90
OPA_VR1_KM69_04	69	KM69_04	90
OPA_VR1_KM69_05	69	KM69_05	90
1107_VR2_KM72_S106	72	S106	90
1107_VR2_KM71_S03	71	S03	90
1107_VR2_KM72_S102	72	S102	90
1107_VR2_KM71_S05	71	S05	90
1107_VR2_KM71_S06	71	S06	90
1107_VR2_KM71_S07	71	S07	90
1107_VR2_KM72_P115	72	P115	0
1107_VR2_ KM72_P109	72	P109	0
1107_VR2_ KM72_P13	71	P13	0
1107_VR2_KM71_P14	71	P14	0
1107_VR2_KM71_P09	71	P09	0
1107_VR2_KM71_P10	71	P10	0
1107_VR2_KM70_X24	70	X24	30
1107_VR2_KM70_X25	70	X25	30
1107_VR2_KM70_X27	70	X27	30
1107_VR2_KM70_X30	70	X30	30
107_VR2_KM71_Z19	71	Z19	45
1107_VR2_KM71_Z21	71	Z21	45
1107_VR2_KM71_Z23	71	Z23	45
UCS tests			
1107_VR2_KM71_P08	71	P08	0
1107_VR2_KM71_P11	71	P11	0
1107_VR2_KM72_P110	72	P110	0
1107_VR2_KM72_P111	72	P111	0
1107_VR2_KM72_S103	72	S103	90
1107_VR2_KM72_S104	72	S104	90
1107_VR2_KM72_S107	72	S107	90
1107_VR2_KM70_X28	70	X28	30
1107_VR2_KM70_X29	70	X29	30
1107_VR2_KM71_Z15	71	Z15	45
1107_VR2_KM71_Z16	71	Z16	45

Tab. 2-2: Tests from Ferrari et al. (2013) considered in the comprehensive analysis and test IDs.

Test results from NAB12-50 (Ferrari et al. 2013)		
Specimen name	Core/Test ID in the report	Orientation to bedding [°]
Oedometer tests		
Opalinus Clay -2	OPA-2	90
Opalinus Clay -20	OPA-20	90
Opalinus Clay -6	OPA-6	90
Opalinus Clay -18	OPA-18	90
Swelling tests		
Opalinus Clay -20	OPA-20	90
Retention Curves		
Opalinus Clay -3	OPA-3	90

A series of Brazilian tests were performed in the context of the testing campaign by Jahns (2013); despite the recognized significance of the tensile strength, such tests are not considered in the proposed analysis. This is due to the fact that the stress state experienced by the material is not completely defined in such type of testing procedure. In such tests the tensile stress is determined in relation to the stress distribution developed inside the sample due to the application of the vertical load; this stress corresponds to the minimum principal stress σ_3 while the maximum principal stress σ_1 can be estimated as $3\sigma_3$; however the principle stress σ_2 is not defined thus the calculation of the p and q cannot be carried out. In addition the pore water pressure is not monitored or controlled thus the analysis in terms of effective stress cannot be performed.Thus the results are not suitable to be used in an analysis based on the calculation of the stress invariants (later defined as q and p') which, on the other hand, requires a careful evaluation of the principal stresses in the tested samples.

The analysis of the geomechanical tests allows the evaluation of the strength, stiffness and deformation properties of Opalinus Clay, thus providing the fundamental requirements for the constitutive modelling of the material.

Together with the performed geomechanical tests, the relevance of the coupled phenomena is assessed through the investigation of the swelling behaviour and of the water retention behaviour (LMS/EPFL). Thus further considerations in relation to the hydro-mechanical coupling effects on to the deformation behaviour of Opalinus Clay can be provided. The understanding of the mechanical and hydro-mechanical response of the material constitutes the base for the determination of the features to be taken into consideration for a suitable constitutive modelling framework development for Opalinus Clay.

3 Diagnostic analysis of the geomechanical data base from the triaxial testing campaign

Several triaxial tests have been carried out by Jahns (2013), and test results have been provided to LMS/EPFL by NAGRA. The tests have been carried out considering different loading orientations with respect to the bedding direction (P=parallel, S= perpendicular, X=30° and Z=45°) thus allowing the investigation of the anisotropic behaviour of Opalinus Clay. The diagnostic analysis comprises the determination and interpretation of the diagnostic plots p'–q, q–ε_a, ε_a–ε_v, Δu–ε_a, where p' and q are the mean effective and the deviatoric stresses respectively which are defined as:

$$p' = \frac{\sigma_1 + 2\sigma_3}{3} - u$$

$$q = \sigma_1 - \sigma_3$$

ε_a and ε_v are the axial and volumetric strains, u is the pore water pressure (pwp) while Δu is the excess pore water pressure. In addition, the analysis considers the evaluation of the results in terms of the deformation mechanism of the material. In order to investigate the constitutive behaviour of Opalinus Clay, the development and evolution of the excess pore water pressure has been analysed.

The interpretation and analysis of the results is performed considering the testing procedure adopted for the triaxial tests; the results of the testing campaign can be strongly dependent on the testing methodology adopted, thus a correct assessment of the results must take into account all the possible limits and uncertainties. The major aspects that will be considered in the diagnostic analysis of the delivered triaxial tests database can be summarized as follows:

- consideration and comments on the testing procedure (control of initial sample conditions, saturation process, consolidation phase, strain rate effect...);
- diagnostic analysis of the results from the triaxial testing campaign (shear phase, evaluation of strength parameters, stiffness, post peak behaviour).

3.1 Analysis of the testing procedure

A suitable and accurate testing procedure is fundamental for the control of the initial conditions of the samples as well as the sample conditions during the test. In the context of this work, particular attention is given to the following:

- Skempton test for saturation check;
- effects of the strain rate during the shearing phase;
- consolidation phase
- quality and reliability of data acquisition.

3.1.1 Skempton test for saturation check

The Skempton test is adopted to evaluate the saturation of the sample during triaxial tests (Skempton 1954). During this test the change in pore water pressure (Δu) is determined as a function of the increment in isotropic confining pressure ($\Delta\sigma_c$) under undrained conditions; the Skempton's coefficient B is expressed as follows:

$$B = \frac{\Delta u}{\Delta \sigma_c}$$

Under the assumption that the solid and fluid are incompressible, the saturation is complete if B approaches 1. Multiple evidence is available which reports a B value lower than 1 for low porosity geomaterials like rocks and shales (Berge 1998; Cook 1999; Hart 2000) where the fluid and grains compressibility play a role; for such reason an appropriate B value has to be found. In order to ensure a traceable and reliable execution of the geomechanical test programme, NAGRA decided to set the minimum B value to 0.8 as a performance indicator for appropriate consolidation and saturation conditions (Jahns 2013). For all tested samples, the Skempton test was done twice with a confining pressure change interval of 0.2 MPa (see Appendix A in Jahns 2013).

The results of test X27 are reported in Figure 3-1. They show that a certain time is needed to reach a Skempton coefficient equal to 0.8. The results reported in the graph highlight the fact that a certain time is required for the complete development of the excess pwp thus the entire triaxial test need to be run at a very slow rate. In this context the evaluation of the correct shearing rate to adopt during the test is of primary significance in order to capture the constitutive behaviour of the material.

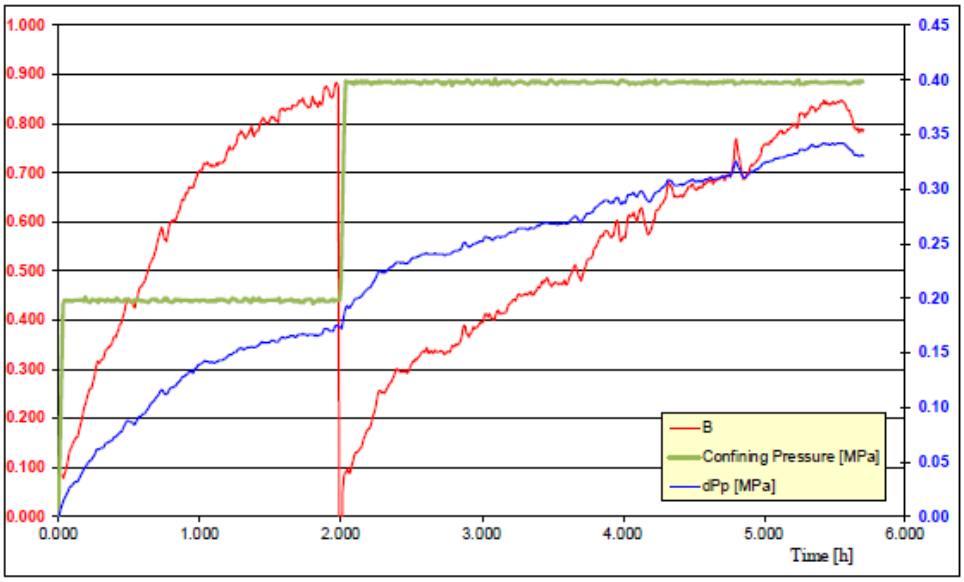

Fig. 3-1: Results of the Skempton test, test X27 (Jahns 2013).

The delay in the measurement of the excess pore water pressure can be due to the characteristics of the device, which may not be able to capture a representative fluid pressure for the entire sample, or to the delay in the pressure transmission to the measuring device (pore water transducer) as well as to the presence of some dead volume in the drainage system between the sample and the pore water transducer. Details about the device and pore fluid system characteristics can be found in Jahns (2013): an overall dead volume of the pore fluid system was calculated between 4.6 and 6 ml; however, in order to provide comparable results, all tests were started at the same piston position of the pore pressure generator (Jahns 2013).

An overall compilation of the Skempton tests (see Jahns, 2013; Appendix A) indicated that the aforementioned performance measure (B=0.8) was reached only in a few cases. Most of the tests suffered from pressure recovery and ongoing deformation in response to the shut-in subsequent to the previous consolidation phase. Table 3-1 gives a survey of the results as reported in Table A-1 of Jahns (2013), together with a brief evaluation of the state of consolidation and saturation during the Skempton test stage.

Tab. 3-1: Results of the Skempton tests after Jahns (2013) / Appendix A.

Test	σ_3 [MPa]	p_w [MPa]	σ'_3 [MPa]	Estimated B-value [-]	Remarks
P09	7.61	3.04	4.57	n.a.	Incomplete saturation
P10	12.61	5.04	7.57	n.a.	Incomplete saturation
P13	22.61	9.04	13.57	n.a.	Incomplete saturation
P14	7.61	3.04	4.57	n.a.	Abrupt change to constant P_f
P109	12.61	5.04	7.57	0.55 / 0.90	Ok
P115	7.61	3.04	4.57	0.65 / 0.95	Ok
S03	12.61	5.04	7.57	n.a.	Consolidation disequilibrium
S05	7.61	3.04	4.57	0.65	Incomplete saturation, followed by abrupt change of P_f after 2nd $\Delta\sigma_c'$
S06	12.61	5.04	7.57	n.a.	Incomplete saturation
S07	22.61	9.04	13.57	n.a.	Consolidation disequilibrium
S102	22.61	9.04	13.57	1.35 / 0.90	Consolidation disequilibrium
S106	7.61	3.04	4.57	n.a.	Incomplete saturation / consolidation disequilibrium
X24	7.61	3.04	4.57	0.80 / 0.90	Drop of P_f after reaching asymptotic value indicates small consolidation disequilibrium
X25	12.61	5.04	7.57	0.95 / 1.1	Only small change in slope toward asymptotic value
X27	22.61	9.04	13.57	0.90 / 0.85	Ok
X30	22.61	9.04	13.57	(0.60) / 0.70	No clear change in slope in 1st $\Delta\sigma_c'$
Z17	22.61	9.04	13.57	n.a.	Consolidation disequilibrium
Z19	7.61	3.04	4.57	n.a.	Incomplete saturation / consolidation disequilibrium
Z21	12.61	5.04	7.57	n.a.	Consolidation disequilibrium
Z23	22.61	9.04	13.57	n.a.	Incomplete saturation

3.1.2 Strain rate effect

In order to investigate the constitutive behaviour of the material by means of undrained triaxial tests, the correct monitoring and recording of the excess pore water pressure (pwp) development is of primary significance. Multiple evidence can be provided from literature (Swan et al. 1986; Al-Bazali et al. 2008) to show the dependency of the strength and pore pressure build up on the strain rate adopted during an undrained triaxial test on shales. The strain rate should be slow enough to allow the measurement of the excess pore water pressure; the evaluation of the correct strain rate can be achieved thanks to the performance of different tests with different strain rates. One should investigate the adequate rate to have the excess pwp read by the system instantaneously, i.e. a further decrease of the strain rate will not lead to the observation of higher pore water pressures.

Different tests at different strain rates and at the same confining pressure have been performed in the context of the considered testing campaign (KM69_01, KM69_02, KM69_03, KM69_04, KM69_05) and the pore water pressure build up during the tests have been recorded.

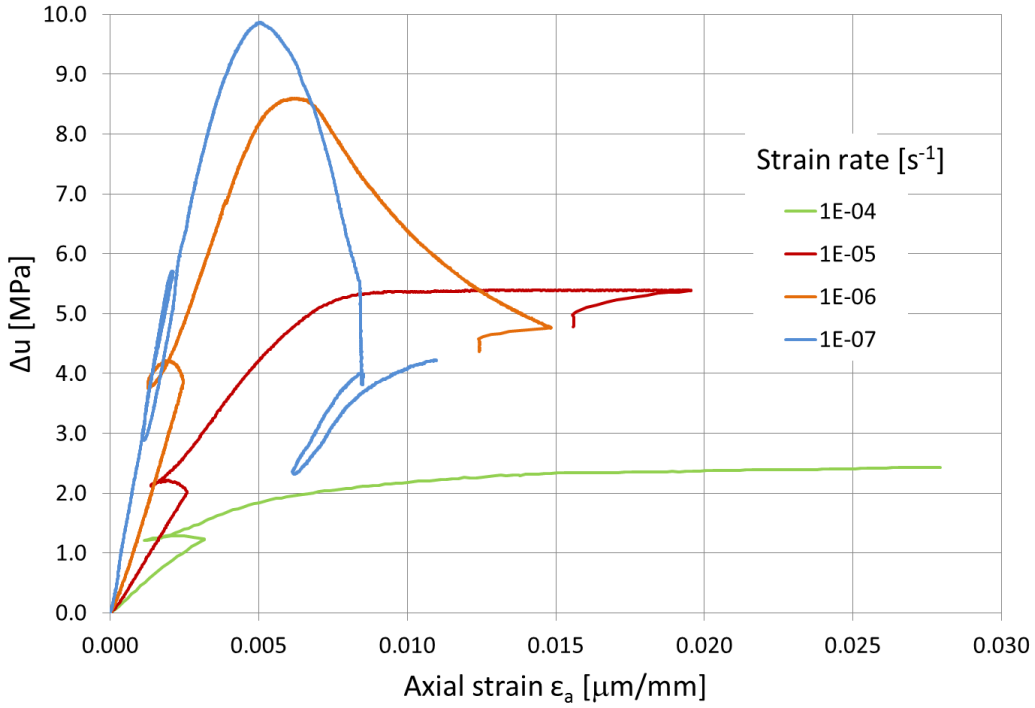

Fig. 3-2: Pore water pressure development during shearing for different strain rates (KM69_01, KM69_02, KM69_03, KM69_05).

The selection of the correct strain rate is fundamental for the correct measurement of the excess pwp development and thus for the evaluation of the effective stress paths followed during the tests. The increase of the measured pore water pressure can be observed with decreasing strain rate.

3.1.3 Consolidation

The CIU (consolidated-undrained with pore water pressure measurement) triaxial test requires the saturation and the consolidation of the sample during an isotropic compression phase, before the shearing phase.

The consolidation process of the tested samples is evaluated together with the saturation phase since the confining stress is applied together with the increasing pore water pressure. As explained in Jahns (2013), the time for the consolidation phase is evaluated using the same criterion considered for the saturation check. Due to the low permeability and the consolidation properties of the material, this criterion might not be suitable to correctly interpret the consolidation process of Opalinus Clay (see Chapter 3.1.1). A more accurate analysis can be achieved considering the settlements versus time curves of the consolidating samples, together with the pore water volume behaviour with time.

The swelling and the consolidation processes and thus the dissipation of the excess pwp manifest with the absorption or expulsion of the pore fluid and with decreasing or increasing deformations of the sample. The swelling/consolidation phase can be assumed to be completed once the previous phenomena stabilize, and settlements and pore fluid volume variations adjust to constant. In this sense, the analysis of deformation vs. time curves and time-pore fluid volume curves is particularly significant.

Selected results from the available database are reported in Figs. 3-3 to 3-6, as an example of the interpretation of the pore water volume vs. time curves and settlements vs. time curves.

Figure 3-3 is related to the P samples; it is possible to observe that, once the target confining and pwp pressures are reached, the pore water volumes keep on increasing, this indicating that the samples are absorbing water and saturating. This phenomenon may or may not be associated with a swelling of the material; a certain swelling is observed only for the sample at the lower confining pressure. The consolidation manifests with a decreasing pore fluid volume and increasing strains (settlements) of the material. Saturation and consolidation of the material are achieved once the pore water volume and the settlements are equalized: this is observed only for the P-sample at a medium confining pressure (P109). Figure 3-4 refers to selected S samples: once the target confinement and pwp are reached almost an immediate decrease of pore fluid volume is observed together with the occurrence of settlements. These are factors indicating that the consolidation is taking place. For the sample consolidating at 22.61 MPa (S102) the pore fluid as well as the settlements seem to stabilize. The time allowed for this sample to consolidate was about 145 hrs (about 6 days); this is an indication of the suitable time to complete the saturation and consolidation phases. The processes of swelling and consolidation seem close to the stabilization also for samples S106 and S03.

Figure 3-5 reports the results of the consolidation analysis for the X samples: an increasing pore fluid volume together with a tendency to swell is observed for the samples at the lower confining pressures (X24 and X25) while the sample at the greatest confining pressure manifests a decreasing pore fluid and increasing settlements thus clearly indicating that the consolidation is taking place. Such processes of swelling and consolidation seem to be almost stabilized for all the X samples in particular for X24. In Figure 3-6 the results for the Z samples are reported; in this case, as already observed for the P samples, the pore water volume going inside the sample is increasing while the samples show a certain swelling. This reveals that the equalization process is not yet concluded.

All the available tests provided by Nagra have been subjected to the analysis; in Tables 3-2 to 3-5 the total confining pressure (σ_3), the pore water pressure (pwp), the effective confining pressure (σ'_3) at which the saturation and consolidation of the material take place and the time allowed for the process to develop (t_{sat+c}) are reported for the P-samples, S-samples, X-samples and Z-samples respectively, together with an evaluation of the achieved saturation and consolidation for each test. In the tables the strain rate at which the subsequent shearing phase takes place is also reported for each test. Based on the analysis of the saturation and consolidation processes, together with the evaluation of the adopted strain rate during shearing, the selection of the most reliable dataset has been performed. The selected tests are highlighted in green colour. The selected database will be further adopted for a more accurate estimation of the strength and stiffness parameters of the Opalinus Clay.

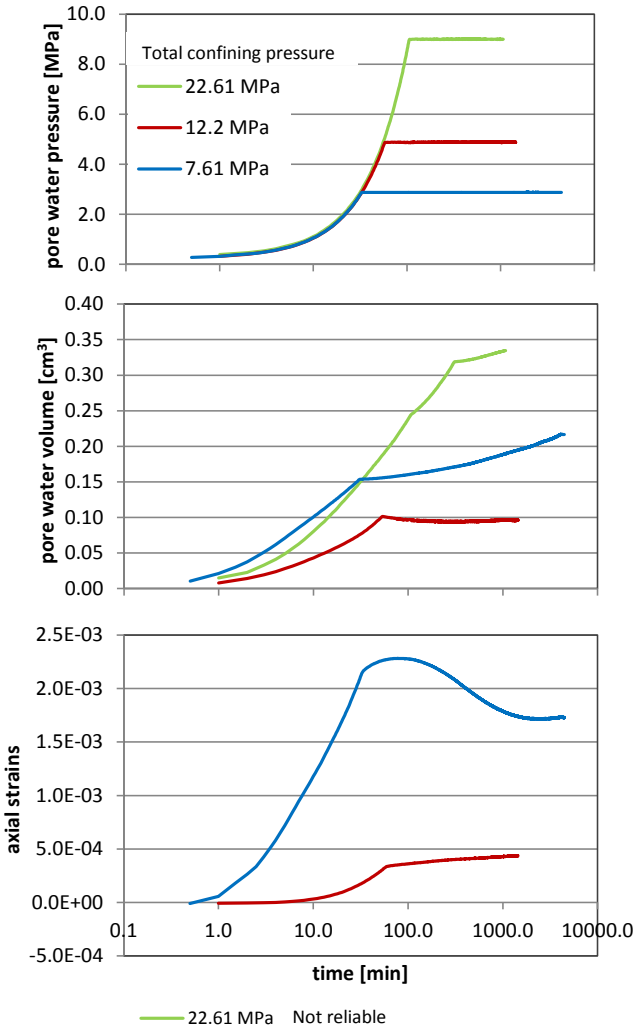

Fig. 3-3: Saturation/consolidation curves for selected P samples (P14 green, P109-red, P115 –blue).

Tab. 3-2: Total confining pressure, pore water pressure, effective confining pressure and time allowed for the consolidation process – P samples.

Test	σ_3 [MPa]	p_w ** [MPa]	σ'_3 [MPa]	t_{sat+c} [hrs]	Saturation state	Consolidation/ swelling state	Strain rate* [s^{-1}]
P115	7.61	2.9	4.7	74.4	ok	no	1E-06
P109	12.2	4.9	7.3	21.1	ok	almost	1E-06
P14	22.61	9.0	13.6	17.8	almost	no	1E-06
P13	22.61	9.0	13.6	68	almost	no	1E-06
P09	7.61	3	4.6	16	no	no	1E-06
P10	12.61	5	7.6	18	almost	no	1E-06

* strain rate during the shearing stage

** corresponds to the initial pore water pressure $p_{w,i}$ (i.e. p_w after the consolidation phase)

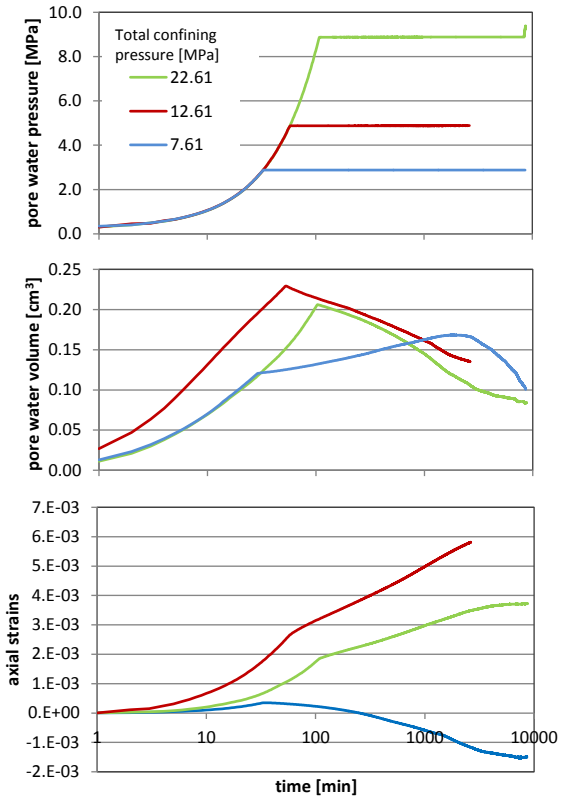

Fig. 3-4: Saturation/consolidation curves for selected S samples (S102-green, S03-red, S106-blue).

Tab. 3-3: Total confining pressure, pore water pressure, effective confining pressure and time allowed for the consolidation process – S samples.

Test	σ_3 [MPa]	p_w ** [MPa]	σ'_3 [MPa]	t_{sat+c} [hrs]	Saturation state	Consolidation/ swelling state	Strain rate* [s^{-1}]
S106	7.61	2.9	4.7	143.3	ok	almost	1E-06
S03	12.61	4.9	7.7	44	ok	almost	1E-06
S102	22.61	9.4	13.2	144.5	ok	ok	1E-06
KM69-2	22.0	9.0	13.0	24	ok	-	1E-05
KM69-3	22.0	9.0	13.0	17	ok	-	1E-06
KM69-4	22.0	1.7	20.3	22	ok	-	1E-04
KM69-5	22.0	9.0	13.0	15	ok	-	1E-07
S05	7.61	3.0	4.6	17	almost	no	1E-06
S06	12.61	5.0	7.6	17	almost	no	1E-06
S07	22.61	9.0	13.6	18	almost	no	1E-06

* strain rate during the shearing stage

** corresponds to the initial pore water pressure pw,i (i.e. pw after the consolidation phase)

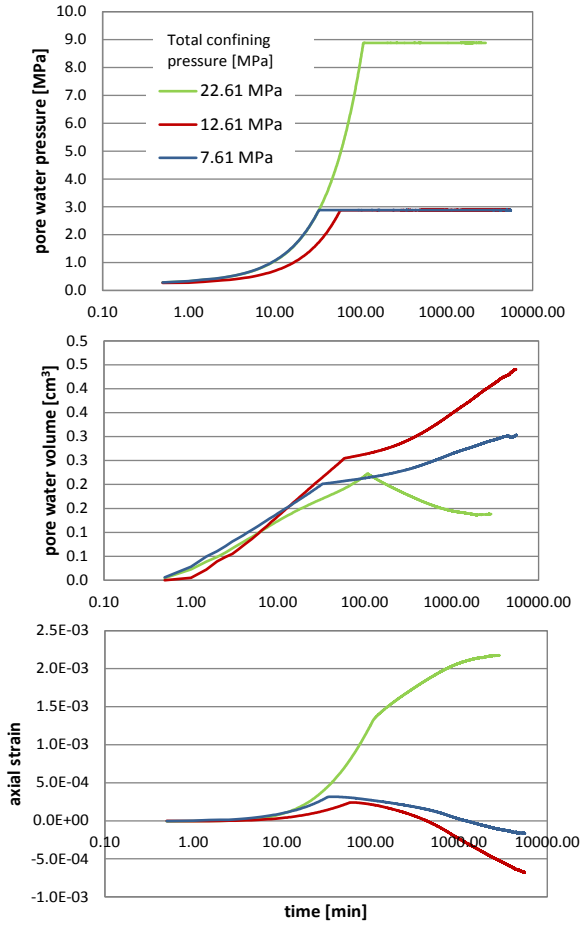

Fig. 3-5: Saturation/consolidation curves for X samples (X27-green, X25-red, X24-blue).

Tab. 3-4: Total confining pressure, pore water pressure, effective confining pressure and time allowed for the consolidation process – X samples.

Test	σ_3 [MPa]	p_w ** [MPa]	σ'_3 [MPa]	t_{sat+c} [hrs]	Saturation state	Consolidation/ swelling state	Strain rate* [s^{-1}]
X24	7.61	2.9	4.7	93	ok	ok	1E-06
X25	12.61	2.9	9.7	92	ok	ok	1E-06
X27	22.61	8.9	13.7	47.5	ok	almost	1E-06
X30	22.61	9.0	13.6	24	ok	ok	1E-06

* strain rate during the shearing stage

** corresponds to the initial pore water pressure pw,i (i.e. pw after the consolidation phase)

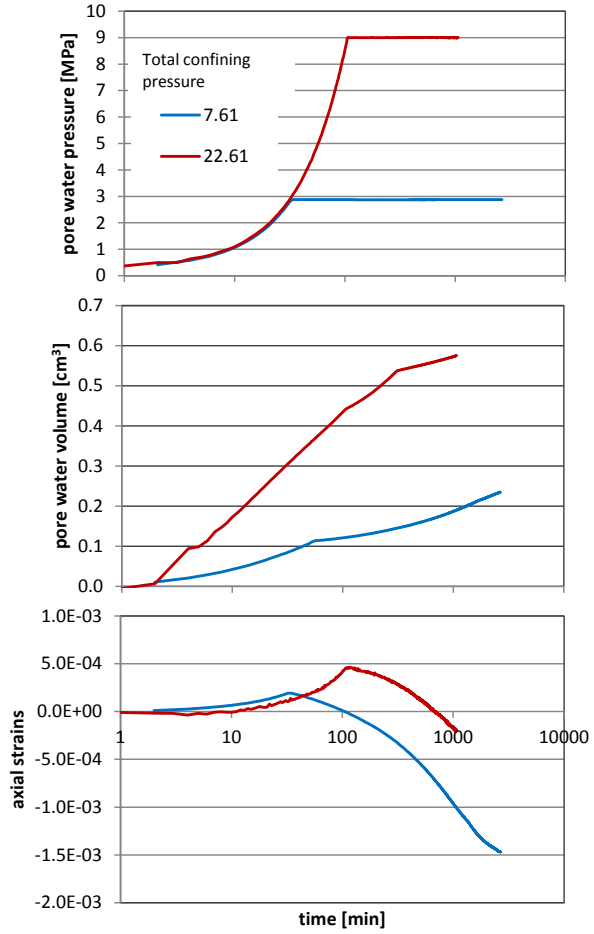

Fig. 3-6: Saturation/consolidation curves for Z samples (Z23-red, Z19-blue).

Tab. 3-5: Total confining pressure, pore water pressure, effective confining pressure and time allowed for the consolidation process – Z samples.

Test	σ_3 [MPa]	p_w ** [MPa]	σ'_3 [MPa]	t_{sat+c} [hrs]	Saturation state	Consolidation/ swelling state	Strain rate [s^{-1}]
Z19	7.61	2.9	4.7	17.8	almost	No	1.0E-06
Z23	22.61	9.0	13.6	44.3	almost	No	1.0E-06
Z21	12.61	5	7.6	80	almost	No	1.0E-06

* strain rate during the shearing stage

** corresponds to the initial pore water pressure pw,i (i.e. pw after the consolidation phase)

3.1.4 Conclusion on quality and reliability of the tests

The test protocols and the execution of the triaxial tests were revisited and analysed. The analysis has been presented in the previous paragraphs and the main observations can be summarised as follows:

- The Skempton B-value (B=0.8 as an indicator for adequate saturation) turned out to be an inadequate performance measure for the assessment of the state of saturation of the test specimen. Nevertheless, the Skempton test has been used an important indicator for the qualification of the test specimen for reliable estimation of strength parameters.
- The strain rate effect has been analyzed; the pore water pressure development is strongly dependent on the rate of shearing of the material. It is important to consider a strain rate deduced from the consolidation stage to ensure the correct acquisition of the pore water pressure; this is required to perform a correct analysis in terms of effective stress and to investigate the volumetric behavior of the material. A series of tests at different strain rate has been performed (KM69_01, KM69_02, KM69_03, KM69_04, KM69_05, see Chapter 3.1.2) and an increase of the excess pwp with a decreasing strain rate is observed thus revealing that a lower rate may allow to better capture the pwp values which might take some time to be recorded by the pore water pressure transducer; this can be due to many reason as addressed in Chapter 3.1.1. A strain rate of 1E-6 s^{-1} has been selected by Jahns (2013) thus all the remaining tests are performed with such rate. Even though the tests with the low strain rates (1E-6 and 1E-7 s^{-1}) seem to converge in terms of the pore pressure development (Fig. 3-2), some uncertainties remain with regard to the suitability of the 1E-6 s^{-1} strain rate; there is yet a difference of about 1 MPa in the excess pwp measurement during the shearing phase, when comparing the tests with the strain rate at 1E-6 and 1E-7 s^{-1}, respectively. As all the tests are run at the same strain rate, this aspect cannot be considered as a quality indicator for the test qualification.

- The saturation and consolidation processes have been analyzed and the importance of the correct performance of these phases has been highlighted. If samples are not completely saturated, suction is developed thus affecting the stiffness and strength of the material. The results of the subsequent shearing phase of the triaxial testing campaign have to be analyzed taking this observation into consideration. On the other end, the consolidation of the material is necessary to have a correct estimation of the pore water pressure recorded during the shearing phase of the triaxial tests and to allow the analysis of the results in terms of effective stresses. A missing or non-complete consolidation of the material might lead to great uncertainties once the interpretation of the results in terms of effective stresses is performed. Again these considerations have to be taken into account for further analysis of the triaxial tests results. The evaluation of the correct development of the swelling/ consolidation phase is an important quality indicator for the perform tests. The evaluation of the correct development of the swelling/consolidation phase is an important quality indicator for the perform tests.

Based on the previous observations in particular related to the analysis of the consolidation phase and Skempton phase reported in Chapters 3.1.1 and 3.1.3, a simple ranking has been elaborated among the available tests to be considered for a more accurate estimation of the strength and stiffness parameters of the Opalinus Clay. The ranking comprises 4 quality levels A – D, level A representing a fully equilibrated sample (full saturation, complete consolidation) and level D representing a poorly equilibrated sample. Table 3-6 displays the Q-levels of the tested samples.

A-level samples were not achieved within the given project constraints (mainly due to the limited overall time for test execution). The recommended tests are tests of level B, comprising P115, P109, P14 for the P samples; S106, S03 and S102 for the S samples; X24 and X25 for the X samples and Z19 and Z23 for the Z samples.

A further selection can be highlighted for numerical modelling purposes: subsequent to the analysis of the saturation, swelling and consolidation processes reported in the previous paragraphs, the tests coded as S03, S102, X24 and X25 are considered the best among the ones available.

Tab. 3-6: Total confining pressure, pore water pressure, effective confining pressure and time allowed for the consolidation process – P samples.

Test	Skempton Test (ref. Table 3-1)	Saturation state (ref. Tables 3-2 to 3-5)	Consolidation/swelling (ref. Tables 3-2 to 3-5)	Q-Level
P09	Incomplete saturation	no	no	**D**
P10	Incomplete saturation	almost	no	**D**
P13	Incomplete saturation	almost	no	**D**
P14	Distorted pwp response	almost	no	**B**
P109	ok	ok	almost	**B**
P115	ok	ok	no	**B**
S03	Consolidation disequilibr.	ok	almost	**C****
S05	Incomplete saturation	almost	no	**C**
S06	Incomplete saturation	almost	no	**D**
S07	Consolidation disequilibr.	almost	no	**D**
S102	Consolidation disequilibr.	ok	ok	**C****
S106	Incomplete saturation/ consolidation disequilibr.	ok	almost	**B**
X24	ok	ok	ok	**B**
X25	ok	ok	ok	**B**
X27	ok	ok	almost	**B**
X30	ok	ok	ok	**C***
Z17	Consolidation disequilibr.			**C**
Z19	Incomplete saturation/ consolidation disequilibr.	almost	no	**D**
Z21	Consolidation disequilibr.	almost	no	**C**
Z23	Incomplete saturation	almost	no	**D**
KM69-05	n.d.	ok see Appendix A	ok see Appendix A	**B**
KM69-03	n.d.	Ok see Appendix A	ok See Appendix A	**B**

* downgraded due to anomalous response during shearing

** downgraded marked increase of pore pressure post peak observed

3.2 Analysis of the test results

A whole database coming from a series of undrained triaxial tests on Opalinus Clay has been subjected to diagnostic analysis. The tests consist of an initial isotropic compression phase which is performed in drained conditions thus allowing the consolidation of the material, followed by the shearing phase. The samples are consolidated at different initial confining pressures thus allowing the shearing of the material at different degrees of overconsolidation.

The diagnostic analysis comprises the determination and interpretation of the diagnostic plots and an evaluation of the results in terms of the deformation mechanism of the material. In the following sections only the plots related to the selected tests (see Chapter 3.1.4) are reported in order to reduce the uncertainties in the challenging understanding of the deformation behaviour of the material; the plots related to the tests that are not reported in this section can be found in appendix A. In the following sections the results of the analysis are reported for the P-samples, S-samples, X-samples and Z-samples separately.

3.2.1 P – Samples

The considered diagnostic plots for the P-samples are reported in Figs. 3-7 to 3-9 and they are related to samples P14, P109 and P115.

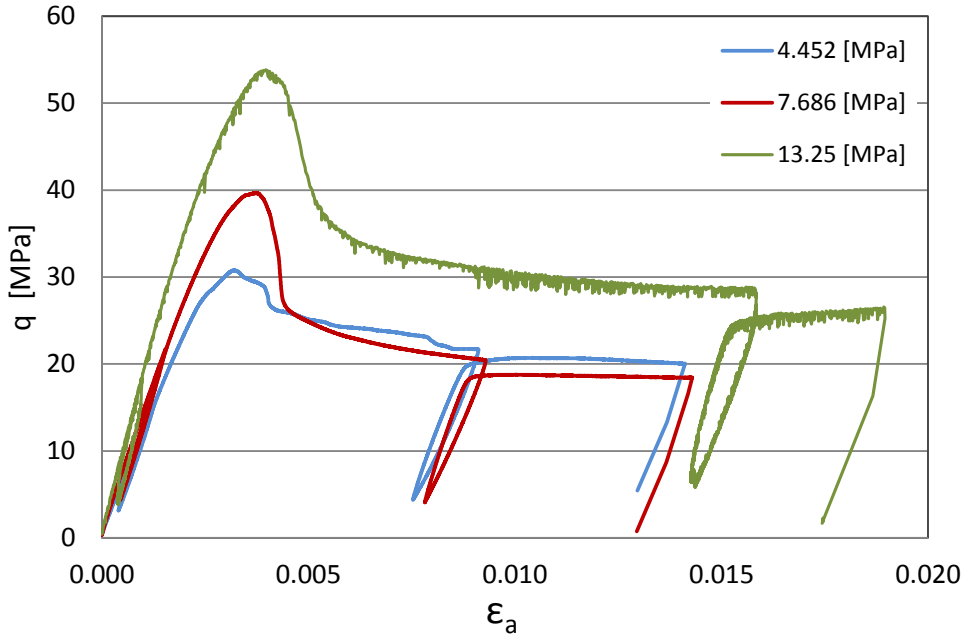

Fig. 3-7: q - ε_a plot for P-samples P14 (green), P109 (red) and P115 (blue).

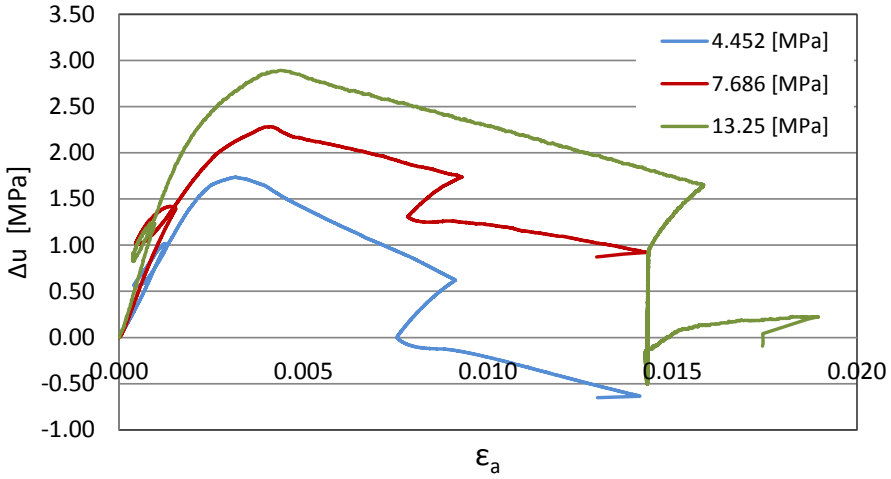

Fig. 3-8: Δu - ε_a plot for P-samples P14 (green), P109 (red) and P115 (blue).

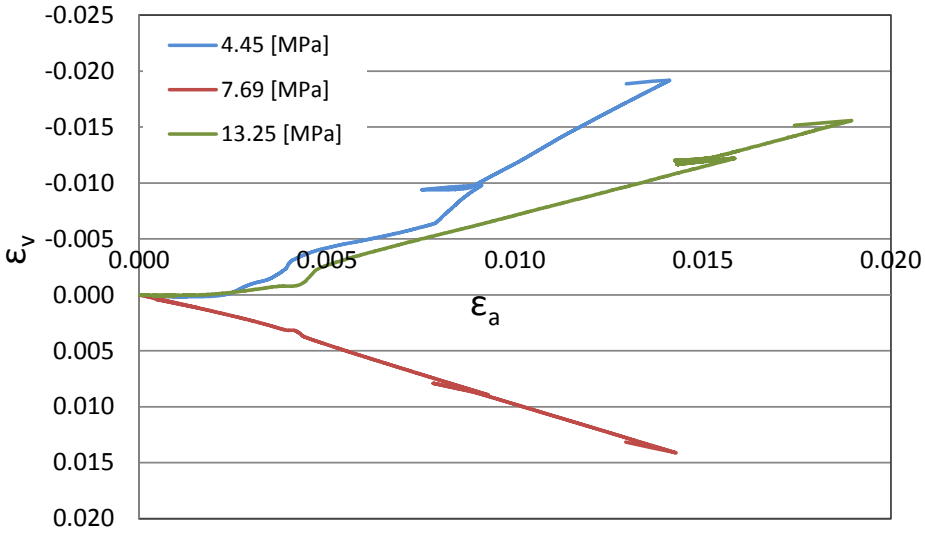

Fig. 3-9: ε_v- ε_a plot for P-samples P14 (green), P109 (red) and P115 (blue).

The deviatoric deformation mechanism can be investigated by the analysis of the previous plots; the shearing phase of the tests is carried out in undrained conditions thus a constant volume would be expected; nevertheless some volumetric strains are recorded in all the tests. The measurement of the radial strains at the middle of the sample is done with a single pin thus the significance of such local measurements is questionable and cannot be considered representative of the whole volumetric deformation mechanism of the sample. Nevertheless, even if not representative, the measured values are significant for this material and they can be taken into consideration to elaborate an analysis on the deformation mode of the material (tendency to dilate or contract). The previous observations limit the accuracy in the analysis of the volumetric behaviour of the material, however some considerations can be made on the bases of the observed results.

Before the peak, where the material has not failed yet, the excess pwp pressure tends toward positive values thus indicating contracting behaviour; once the peak is reached the material experiences a brittle failure and softening while the excess pwp tends to decrease indicating a dilatant behaviour. The volumetric strains seem to confirm this observation since an increasing volume (negative volumetric strains) is observed for two of the three tests performed. Nevertheless, the most commonly observed failure mechanisms of P-samples is axial splitting along the bedding planes, thus the dilatant behaviour individualised by the analysis of the radial strain measured by the single pin in the centre of the sample can be associated to such a failure mode. On the other end a decreasing volume is observed for the test performed at the medium confining stress, so no clear conclusion on the volumetric behaviour can be made.

A further analysis can be developed considering the q-p' plot. In order to highlight the excess pwp development the same initial starting point can be considered shifting the total stress path (p*) toward the effective one (p'); in this way the effect of a non-correct estimation of the excess pwp can be better considered together with the possible consequences in the estimation of the strength parameters.

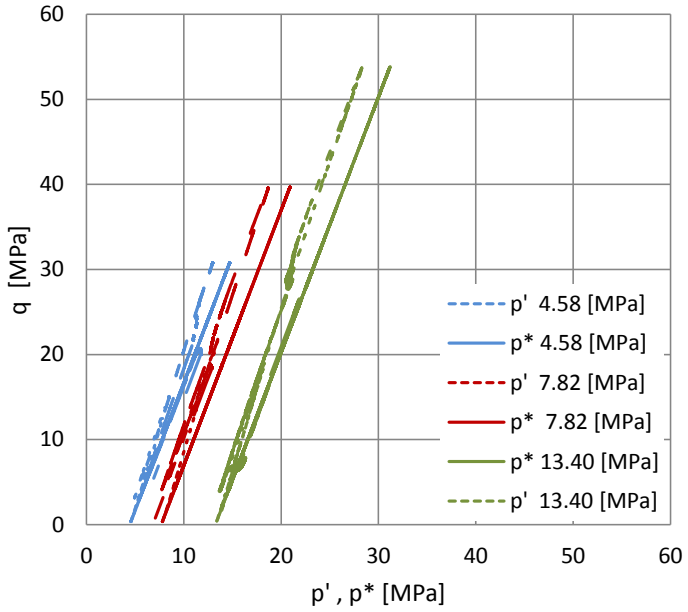

Fig. 3-10: q- p', p* plot for P-samples P14 (green), P109 (red) and P115 (blue).

The derivation of the stress path in terms of effective stress requires the correct estimation of the excess pore water pressure. If a higher positive excess pwp is expected (contracting behaviour), failure surface moves toward the left and the current estimation is on the safe side (Fig. 3-11a). If negative excess pwp is expected (dilatant behaviour), the ultimate state moves toward the right side (Figure 3-11b).

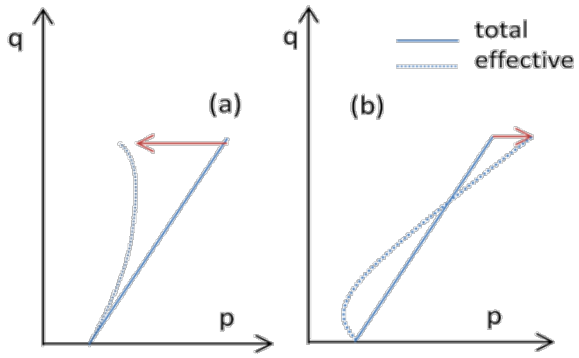

Fig. 3-11: Effective stress path in relation to the excess pore water pressure development.

3.2.2 S – Samples

The considered diagnostic plots for the S-samples are reported in Figs. 3-12 to 3-14 and they are related to samples S102, S03 and S106.

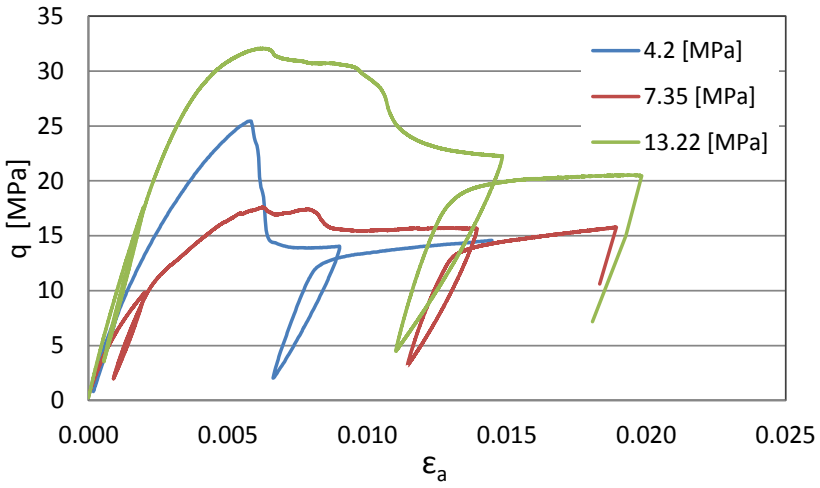

Fig. 3-12: q - ε_a plot for S-samples S102 (green), S03 (red) and S106 (blue).

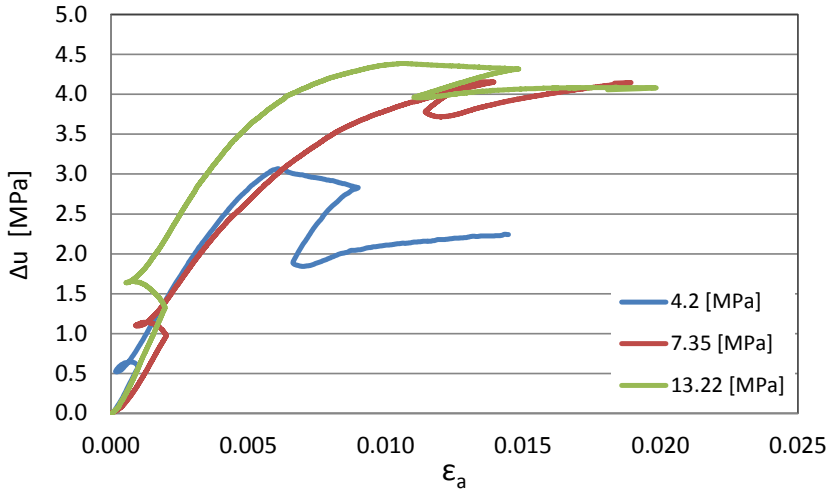

Fig. 3-13: Δu - ε_a plot for S-samples S102 (green), S03 (red) and S106 (blue).

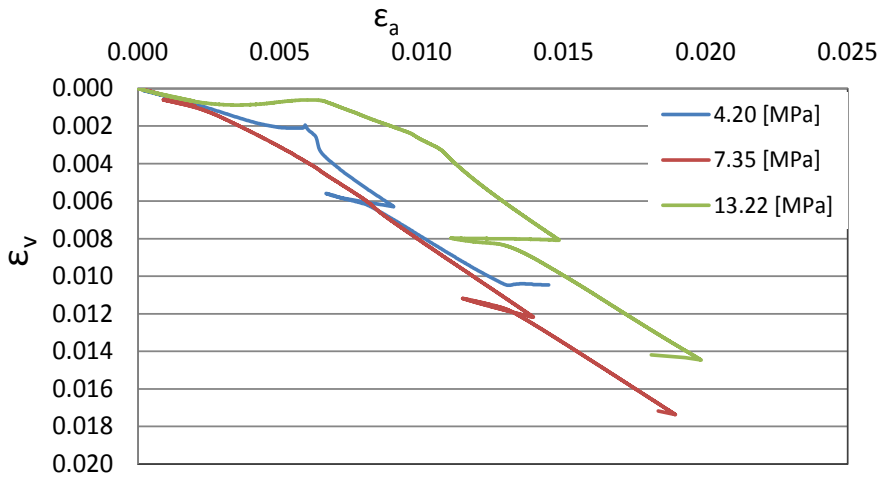

Fig. 3-14: ε_v- ε_a plot for S-samples S102 (green), S03 (red) and S106 (blue).

Before the peak, where the material has not failed yet, the excess pwp pressure tends toward positives values thus indicating contracting behaviour and hardening; while after peak the curves seems to remains almost constant and no relevant excess pwp are observed which means that the material neither contract or dilates. Nevertheless the volumetric strains seem to reveal contracting post peak behaviour.

The q-p' plot is reported in Fig. 3-15 if higher excess pore water pressures are expected, a shift of the effective stress paths toward the origin is also expected. However the current estimation is toward the safe side since respect to the case in which the failure surface would be shift toward the origin.

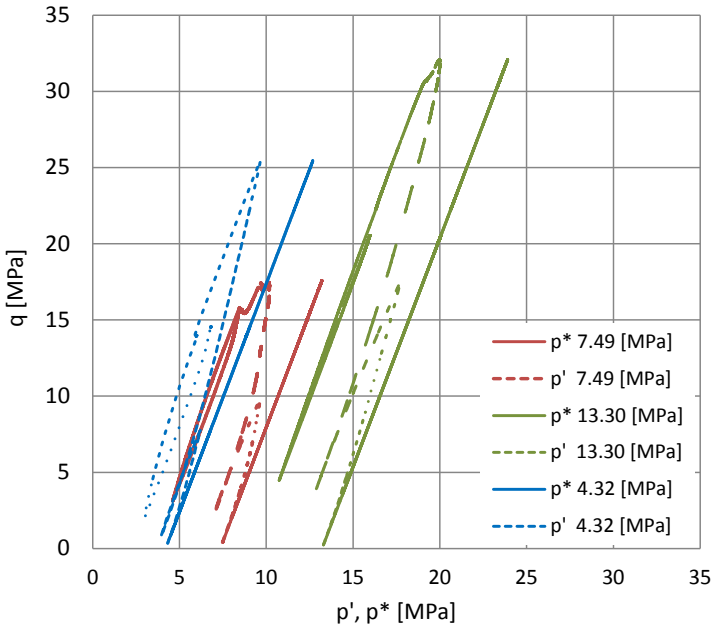

Fig. 3-15: q- p', p* plot for S-samples S102 (green), S03 (red) and S106 (blue).

3.2.3 X – Samples

The considered diagnostic plots for the X-samples are reported in Figs 3-16 to 3-18, they are related to samples X25 and X24.

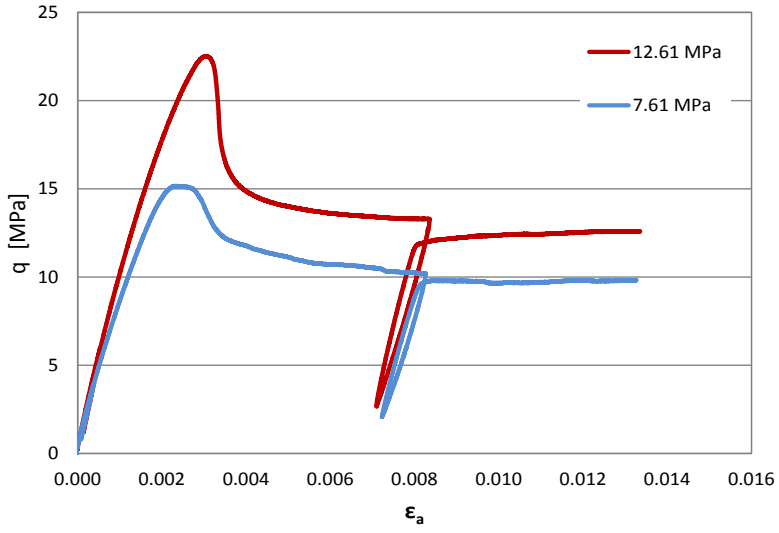

Fig. 3-16: q - ε_a plot for X-samples X25 (red) and X24 (blue).

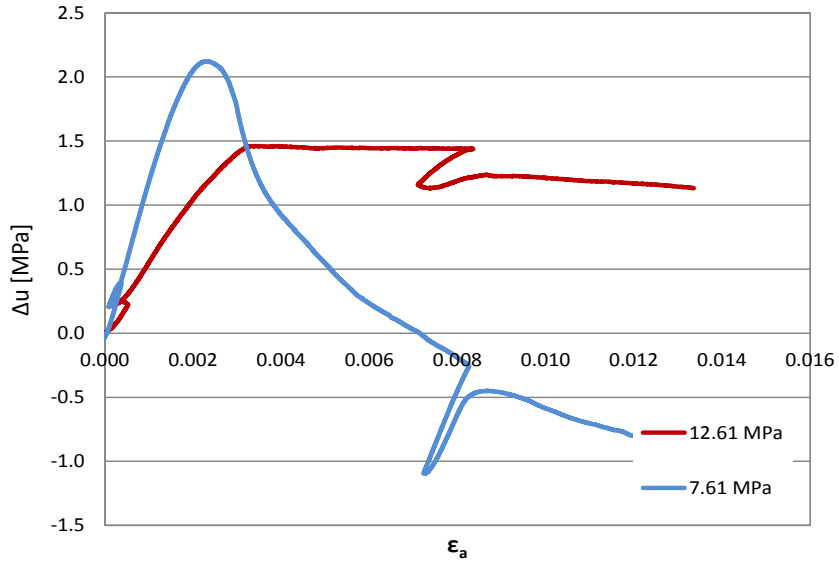

Fig. 3-17: Δu - ε_a plot for X-samples X25 (red) and X24 (blue).

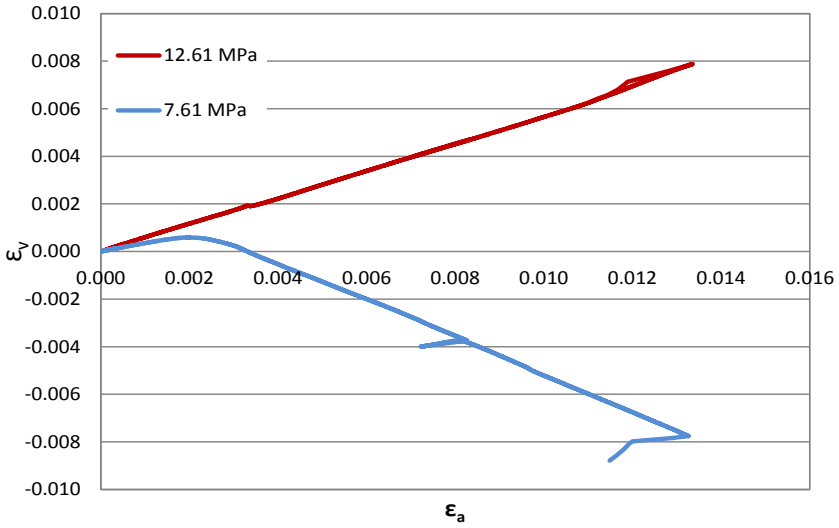

Fig. 3-18: ε_v- ε_a plot for X-samples X25 (red) and X24 (blue).

The sample tested at the two highest confining stresses reveals a contractant behaviour where positive excess pwp are developed and increasing volumetric strains are observed. On the other hand the sample at the lowest confining pressure presents a clear tendency to dilate with a great decrease in the excess pwp which reach negative values together with the occurrence of negative volumetric strains.

The p-q plot for the X samples is reported in Fig. 3-19.

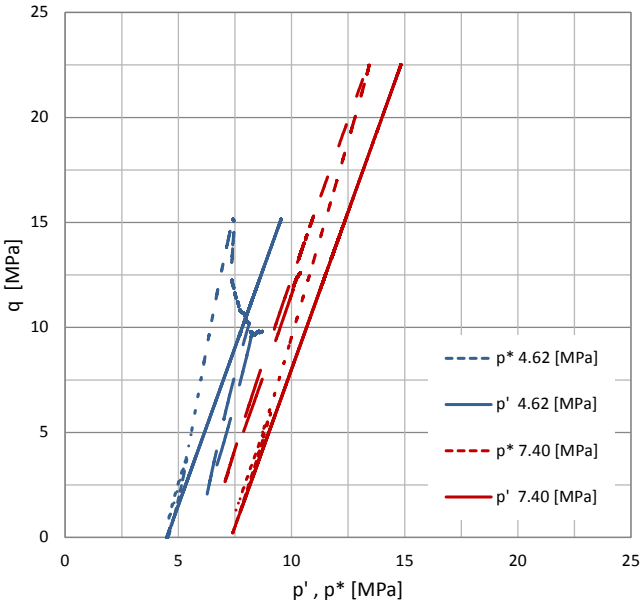

Fig. 3-19: q- p', p* plot for X-samples X25 (red) and X24 (blue).

3.2.4 Z – Samples

The considered diagnostic plots for the Z-samples Z23 and Z19 are reported in Figs. 3-20 to 3-22.

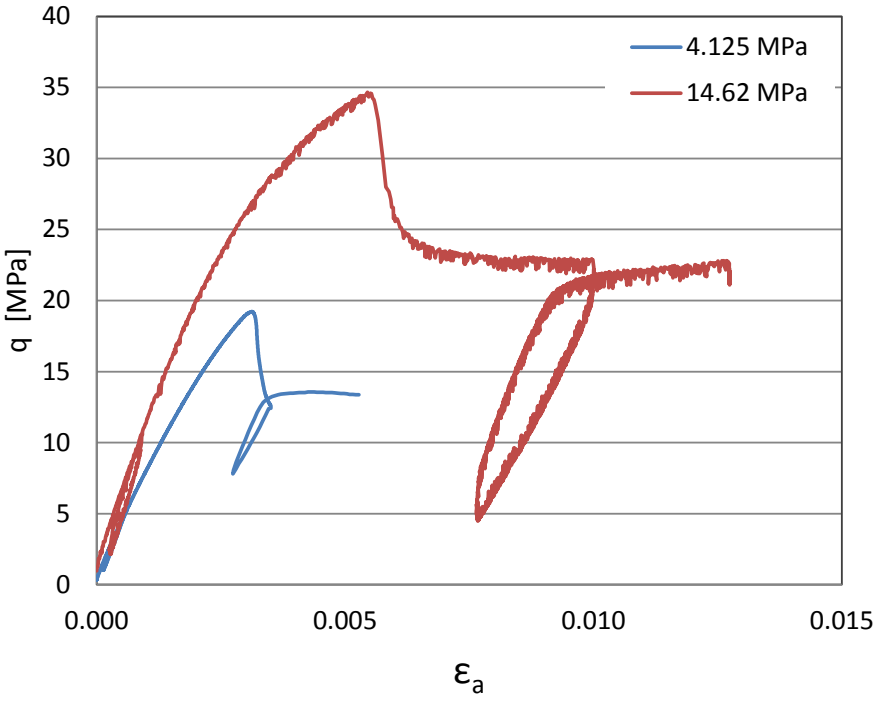

Fig. 3-20: q - ε_a plot for Z-samples Z23 (red) and Z19 (blue).

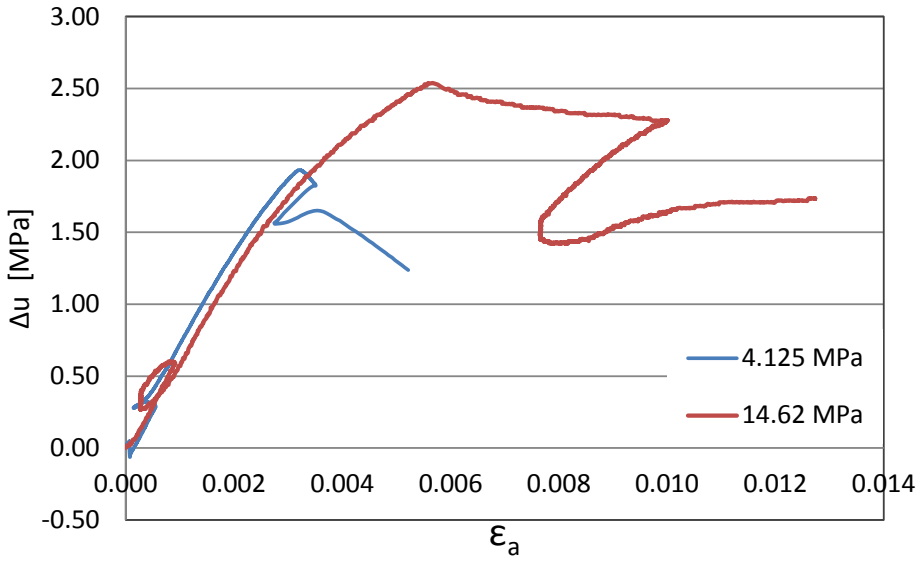

Fig. 3-21: Δu - ε_a plot for Z-samples Z23 (red) and Z19 (blue).

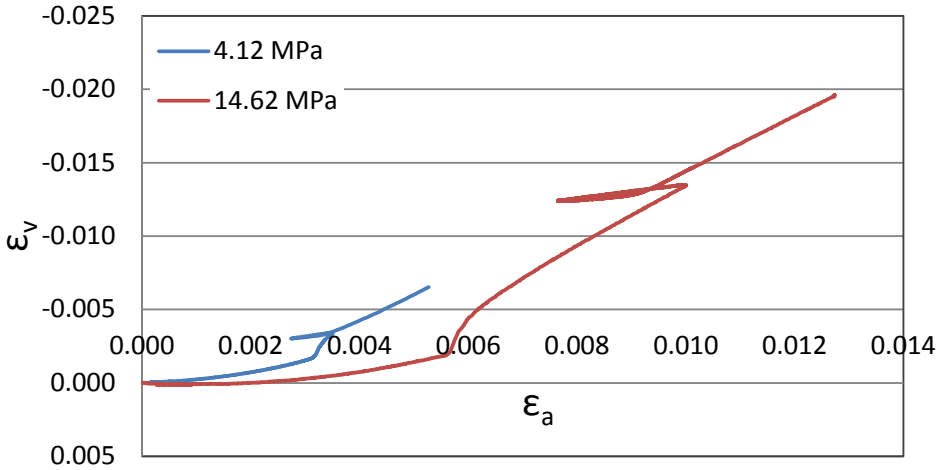

Fig. 3-22: ε_v- ε_a plot for Z-samples Z23 (red) and Z19 (blue).

As in the case of the previous tests, the pre-peak phase is related to the development of positive values of excess pwp which indicate contracting behaviour. On the other end the post peak behaviour is related to more or less constant values pore water pressure while the volumetric behaviour reveals dilatancy of the material. The p-q plot for the Z samples is reported in Fig. 3-23.

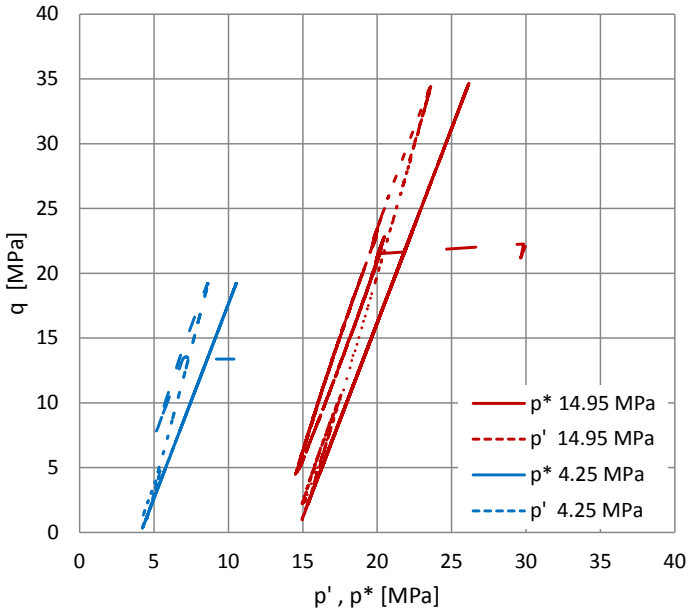

Fig. 3-23: q- p', p* plot for Z-samples Z23 (red) and Z19 (blue).

As observed in Figs. 3-7, 3-12, 3-16 and 3-20, the brittle failure and the softening after peak before reaching the ultimate state can be highlighted for all the samples and no clear relation between the post peak behaviour and the confining stress level can be observed. Figs. 3-8, 3-9, 3-13, 3-14, 3-17, 3-18, 3-21 and 3-22 give an indication on the volumetric behaviour of the tested material. The CIU triaxial tests analysed should highlight constant volume conditions while volumetric strains are recorded; this might be due to the local measurements of the radial strains taken by means of a single pin and which cannot be considered representative of the whole volumetric behaviour of the samples from a quantitative point of view; nevertheless the entities of the volumetric strains recorded are quite significant and they can still give an indication on the qualitative volumetric behaviour of the material. Previous observations highlighted some issues related to the evaluation and measurement of the excess pwp. The non-accurate readings of the values of the excess pwp may lead to errors in the final interpretation of the constitutive behaviour of the material.

3.3 Strength parameters

All the available datasets have been taken into consideration for the determination of the strength parameters for Opalinus Clay. The analysis of the saturation and consolidation phases highlights that some tests are performed without reaching the complete saturation of the samples; as a consequence the shearing phase takes place in partially saturated condition (i.e. suction is developed) resulting in an apparent increase of the shear strength and the stiffness of the material (see further). The strength parameters have been determined based on the entire available dataset despite the unsuccessful saturation and consolidation processes in some tests. Subsequently, only the selected database has been analysed and used for a further estimation of the strength parameters.

In the following sections the estimation of the parameters based on the whole available dataset is initially reported. The intercept cohesion and shear shearing resistance angle for the Mohr-Coulomb criterion are derived directly from the parameters a and M which define the lines characterizing the peak strength condition and the ultimate strength condition on the p'-q plane. The comparison of the results coming from the analysis of the whole dataset and of the selected once allows highlighting the fact that if the saturation is not achieved and the shearing is performed under certain suction, the estimation of the parameters can be affected in a significant way.

The graphs representing the peak strength condition and the ultimate state condition in the p'-q plane for each loading orientation is reported in Figs. 3-24 to 3-27; the whole database is reported together with the selected dataset for the P-samples, S-samples and X-samples while only two complete triaxial tests for the Z-samples were available in the database thus no further selection is performed in this case.

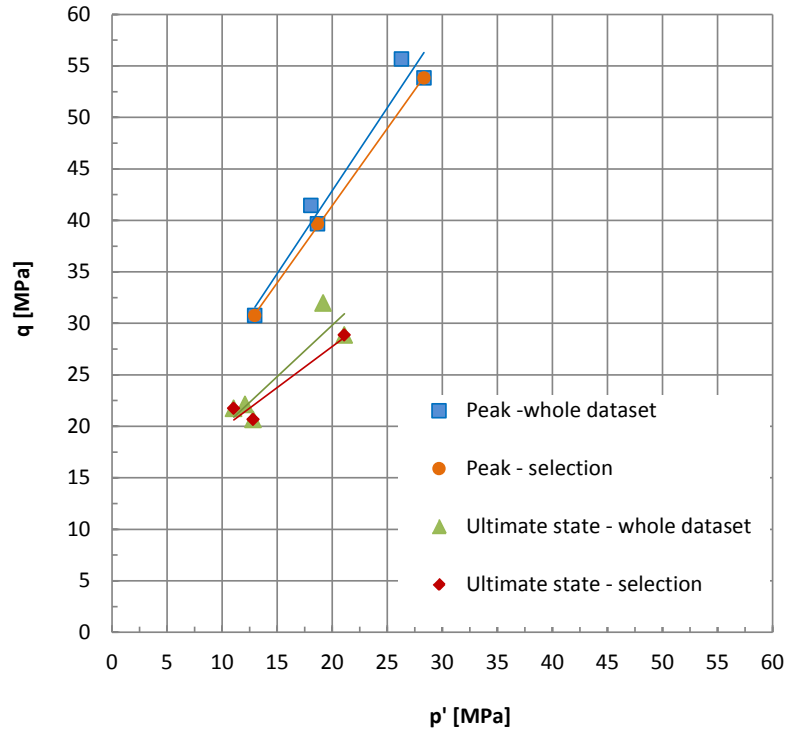

Fig. 3-24: Peak and ultimate state conditions - P samples.

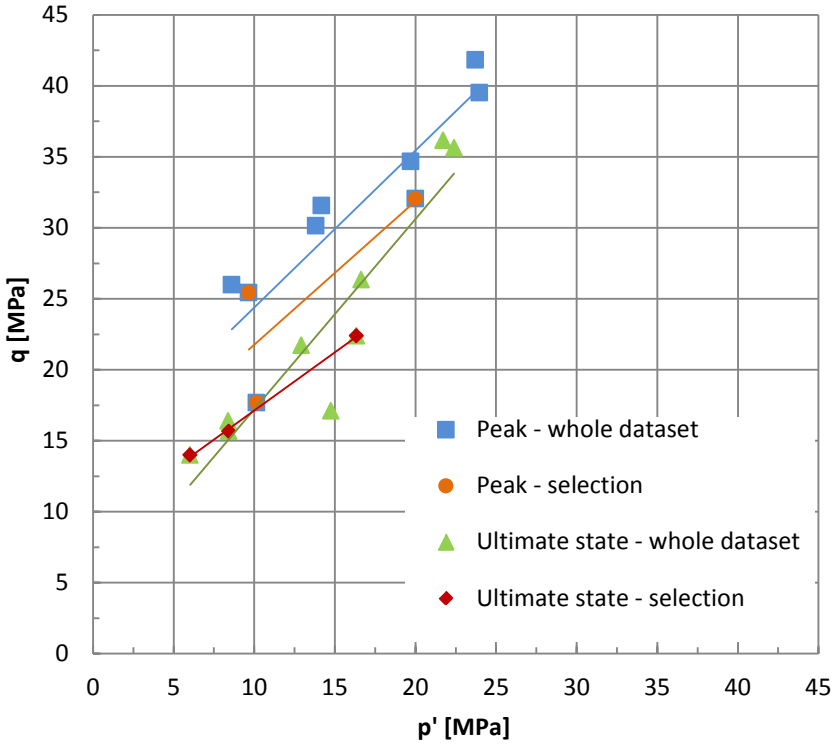

Fig. 3-25: Peak and ultimate state conditions - S samples.

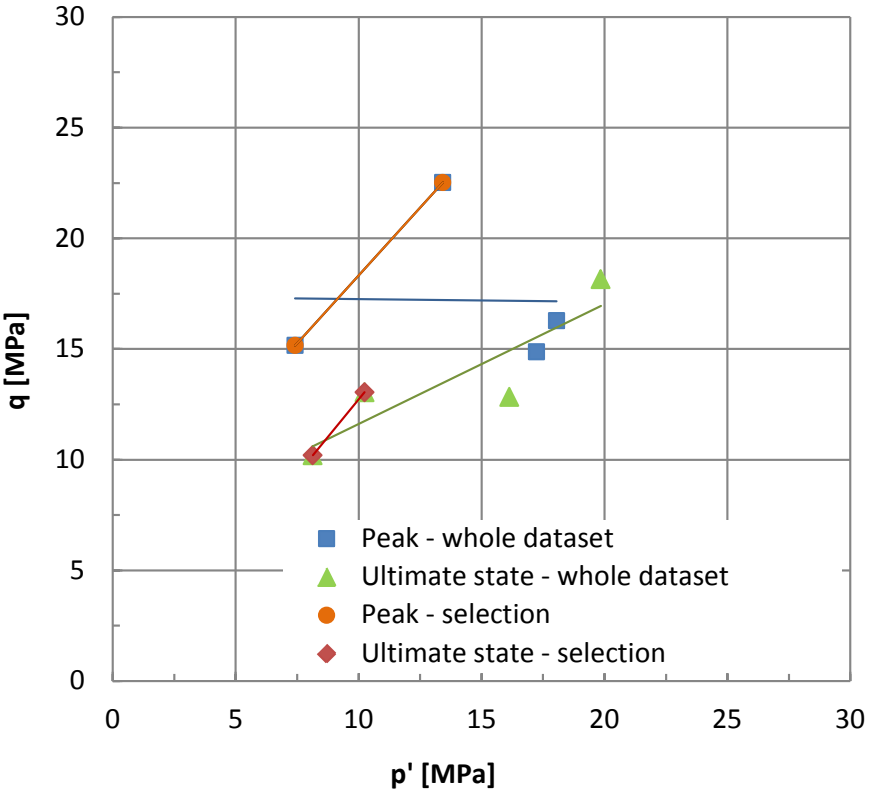

Fig. 3-26: Peak and ultimate state conditions - X samples.

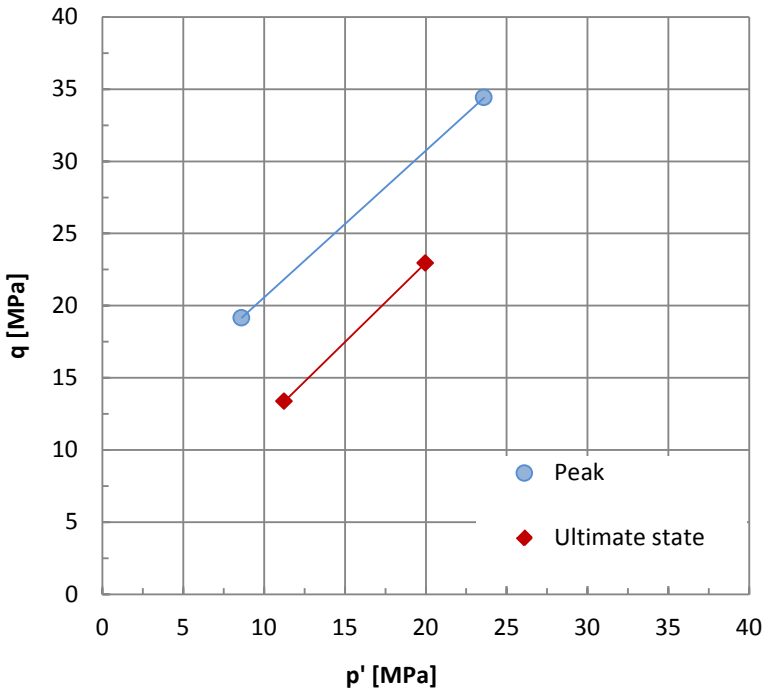

Fig. 3-27: Peak and ultimate state conditions - Z samples.

The values at the peak and at the residual states in the p'-q plane are linked to the corresponding c' and φ' values for the Mohr-Coulomb representation according to the following relationships:

$$c' = a\frac{\tan\varphi'}{M}$$

$$\varphi' = \sin^{-1}\left(\frac{3M}{6+M}\right)$$

where M and a are the slope and the intercept of the lines in the p'-q plane.

The strength parameters derived from the p'-q planes and the corresponding parameters for the Mohr-Coulomb representation are reported in Table 3-7 for the three loading orientations; the parameters derived from the whole database as well as those derived from the selected dataset are distinguished.

Tab. 3-7: Strength parameters.

	a_{peak} [MPa]	M_{peak} [-]	ϕ'_{peak} [°]	c'_{peak} [MPa]	a_{cs} [MPa]	M_{cs} [-]	ϕ'_{cs} [°]	c'_{cs} [MPa]
Whole database								
P-samples	10.70	1.61	39.4	5.5	9.83	1.00	25.4	4.7
S-samples	13.4	1.1	27.7	6.4	3.8	1.34	33.2	1.9
X-samples	17.4	-0.0125	-0.4	8.7	6.2	0.54	14.4	2.9
Z-samples	10.4	1.02	25.8	4.9	1.0	1.09	27.6	0.5
Selection								
P-samples	11.5	1.50	36.8	5.7	11.8	0.80	20.6	5.6
S-samples	11.7	1.01	25.6	5.5	8.9	0.82	21.2	4.2
X-samples	6.1	1.2263	30.6	2.9	0.8	1.35	33.5	0.4

The comparison between the strength parameters obtained from the whole dataset and from the selected one for the P-samples and S-samples is reported in Figs. 3-28 and 3-29.

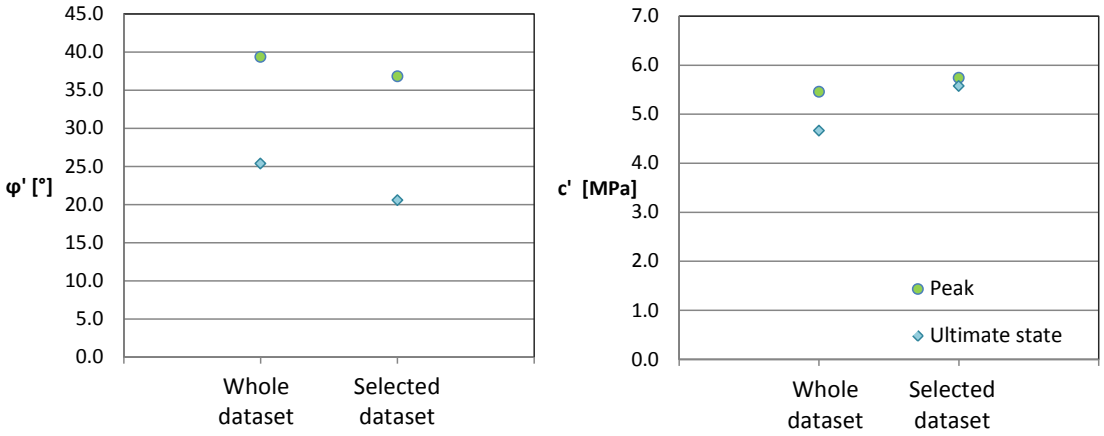

Fig. 3-28: Comparison between the strength parameters obtained from the whole dataset and from the selected one for the P-samples.

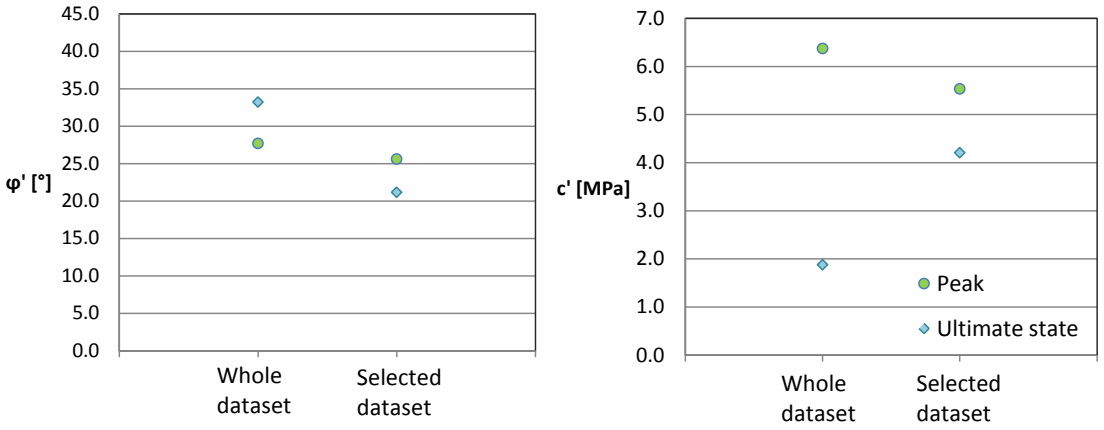

Fig. 3-29: Comparison between the strength parameters obtained from the whole dataset and from the selected one for the S-samples.

The selection of the most reliable tests allows a greater accuracy in the evaluation of the strength parameters; nevertheless the determination of such parameters has to be interpreted in the light of the observations reported in Chapter 3.1. The values of the cohesion reported in the previous table might be influenced by the missing accuracy in the acquisition of the excess pore water pressures since a translation of the peak and ultimate conditions can be observed along the p' axis when greater or lower values of pore water pressure are expected. On the other end, important effects on the determination of the strength parameters can be related to the non-complete saturation process thus the material is tested in unsaturated conditions.

In the light of the analysis of the isotropic compression phase (consolidation), the S and X samples have shown that the swelling/consolidation phase can be assumed to be almost completed compared to the P and Z samples, thus the estimation of the strength parameters can be considered sufficiently robust while a higher uncertainty is related to the determination of the strength parameters for the P and Z samples where the considered saturation and consolidation time has been considerably reduced and the saturation/consolidation processes may not be completed.

3.4 Stiffness parameters

The stiffness parameters for the Opalinus Clay from Schlattingen have been initially determined based on the triaxial tests provided. The Young modulus for the tested samples has been estimated on the first loading-unloading cycle of the q-ε_a curve thus avoiding encountering any irreversible process like hardening or closure of micro-fractures.

The elastic modulus has been calculated on an unloading path as:

$$E = \frac{\Delta q}{\Delta \varepsilon_a}$$

as represented in Fig. 3-30.

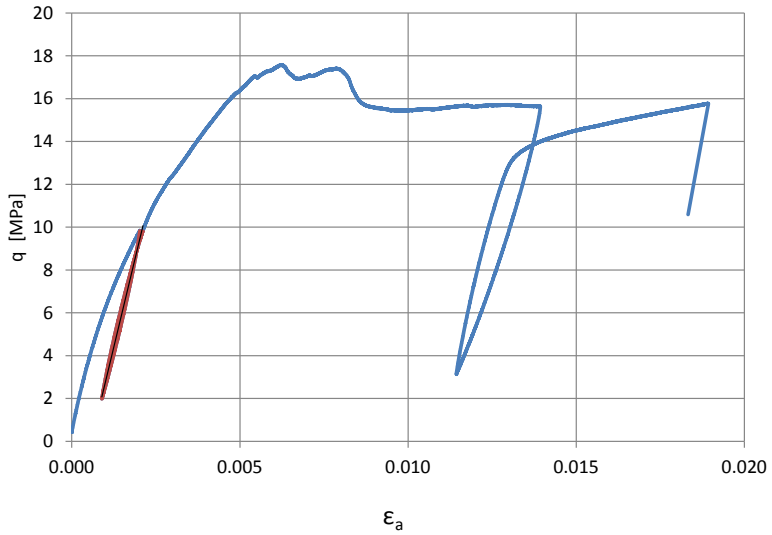

Fig. 3-30: Estimation of the elastic modulus from q-ε_a curve.

It has to be taken into account that, since the test is undrained, the elastic modulus derived is the undrained elastic modulus[1] E_u which in case of linear elasticity can be related to the drained elastic modulus thanks to the following relationship:

$$E = \frac{E_u 2(1+\nu)}{3}$$

[1] The deviatoric component of the elastic response of the material can be written in terms of effective stress as: $\delta q'/\delta\varepsilon_q = 3G'$ where $G'=E/[2(1+\nu)]$. The same relationship applies in terms of total stress for undrained conditions: $\delta q/\delta\varepsilon_q = 3G_u$. The deviatoric stress q is not affected by the drainage conditions: q=q'. Consequently, the shearing, or change in shape of the soil $\delta\varepsilon_q$ is identical in the two cases. Theoretically no change in volume is expected in undrained conditions. Thus K_u tends to infinity, which implies that $\nu \rightarrow 0.5$ and $G_u=E_u/3$. Equating $G'= G_u$ we obtain $E/[2(1+\nu)]=E_u/3$ and thus the relationship used in the report to link the drained and undrained elastic moduli. Note that these considerations are based on the assumption that the Biot coefficient B=1 (incompressible grains).

In order to evaluate the drained elastic modulus, a good estimate of the Poisson ratio is required. The Poisson's ratio ν cannot be derived from the same stress range of the q-ε_a curves as the undrained Young's modulus since the samples are theoretically not experiencing change in their volume (CU triaxial test).

In order to have an estimate of the Poisson ratio for the tested material a series of UCS tests reported in Jahns (2013) have been considered and analysed; the Poisson ratios have been calculated on the reloading part of the hysteresis loop of the $\varepsilon_r - \varepsilon_a$ curve as shown in Fig. 3-31.

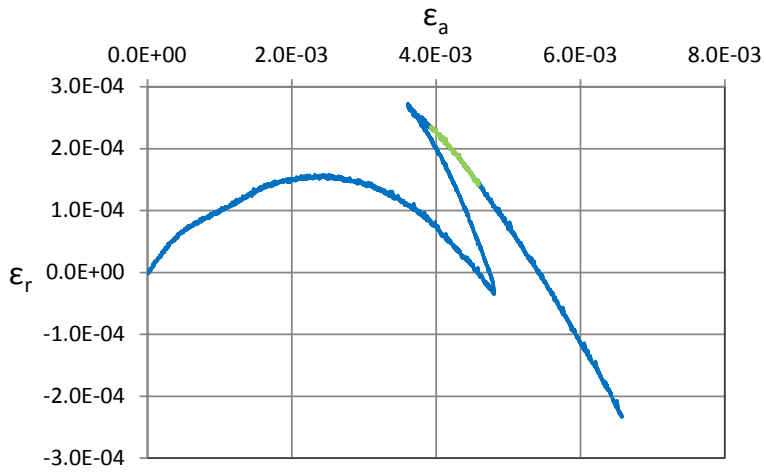

Fig. 3-31: Estimation of the Poisson's ratio from $\varepsilon_r - \varepsilon_a$ curve.

In the UCS tests both the radial and axial strains have been monitored thus the Poisson ratio can be calculated as follows:

$$\nu = -\frac{\Delta\varepsilon_r}{\Delta\varepsilon_a}$$

It has to be stated that the UCS tests are run in unsaturated conditions, the presence of suction in the material have important effects on the mechanical properties of the material. According to the previous statement the Poisson ratios determined from the UCS have to be seen as an underestimation of the real values. In any case, the values derived highlight the typical anisotropic behaviour of Opalinus Clay. This aspect will be further discussed in Chapter 4, where the hydro-mechanical couplings will be considered.

The values of the Poisson ratio determined from the UCS tests and the representative Poisson ratio assumed taking into account the under-estimation due to the unsaturated conditions of the UCS test are reported Table 3-8. The values of the E_u derived from the triaxial tests and the calculated values of the drained elastic modulus E are reported in Table 3-9 in relation to the effective confining pressure.

Tab. 3-8: Poisson's ratio derived from UCS tests.

Samples	$\nu_{from\ UCS\ curves}$	$\nu_{assumed}$
P samples	0.22	0.25
	0.52*	
	0.25	
	0.18	
S samples	0.1	0.14
	0.08	
	0.14	
X samples	0.16	0.16
	0.13	
Z samples	0.21	0.23
	0.23	

* Not representative of the elastic behaviour of the material

Tab. 3-9: Elastic modulus derived from triaxial tests.

Samples	Effective confining pressure [MPa]	E_u [MPa]	E [MPa]
P samples	4.5	14009	11954
	7.7	15616	13326
	13.2	20139	17185
S samples	4.2	8089	6255
	7.3	6566	5078
	13.2	9639	7454
X samples	4.5	10410	8050
	7.7	11811	9134
Z samples	4.1	9211	7676
	14.6	11460	9550

The undrained elastic moduli determined from the analysed triaxial testing campaign in relation to the respective confining pressure are reported in Fig. 3-32 while the calculated drained elastic modulus is reported in Fig. 3-33.

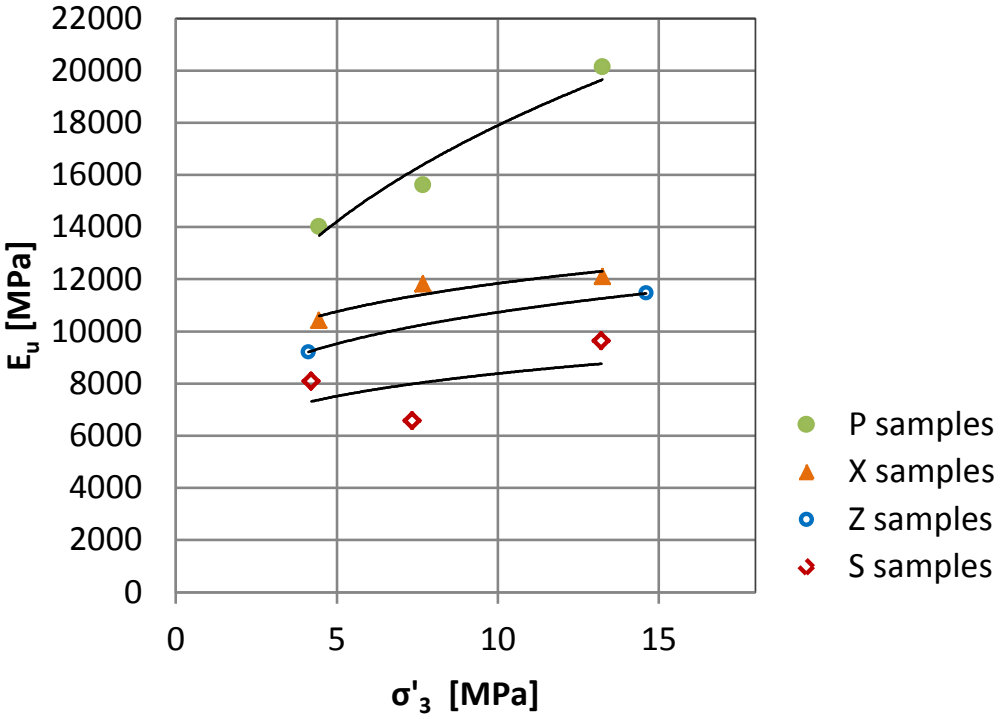

Fig. 3-32: Undrained elastic moduli as a function of effective confining stress.

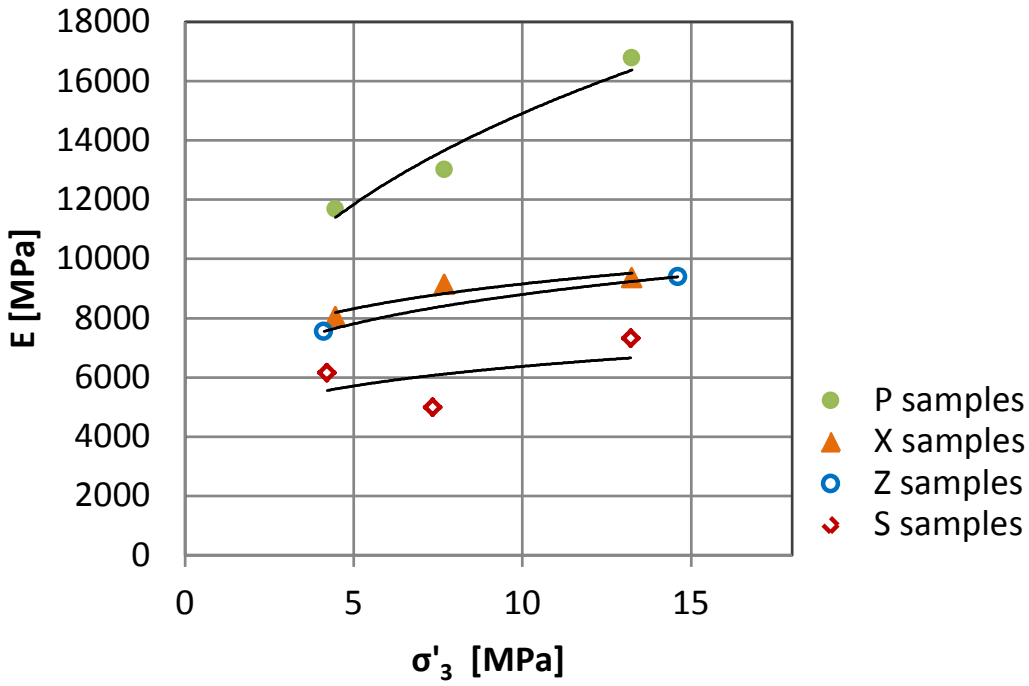

Fig. 3-33: Drained elastic moduli as a function of effective confining stress.

The dependence of the elastic moduli on the confining pressure is observed together with the anisotropic characteristics of the materials. Considerably higher stiffness is observed for the P samples, while the S samples show the lowest stiffness. If an interpolation with a power low is considered for each loading orientation, the following expressions are obtained, linking the stiffness of the material to the corresponding confinement:

$E = 6930\ (\sigma_3')^{0.33}$ for P-samples

$E = 6659\ (\sigma_3')^{0.14}$ for X-samples

$E = 5916\ (\sigma_3')^{0.17}$ for Z-samples

$E = 4431\ (\sigma_3')^{0.16}$ for S-samples

where σ_3' is the effective confining pressure.

Previous investigations conducted on some Opalinus Clay samples from Schlattingen and reported in Ferrari et al. (2012) have highlighted the dependency of the oedometric modulus on the stress level. The results of some high pressure oedometric tests on Opalinus Clay samples oriented perpendicularly to the bedding direction (S-samples) are reported in Fig. 3-34 here the dependency of the Oedometric modulus on the vertical stress acting on the sample can be highlighted.

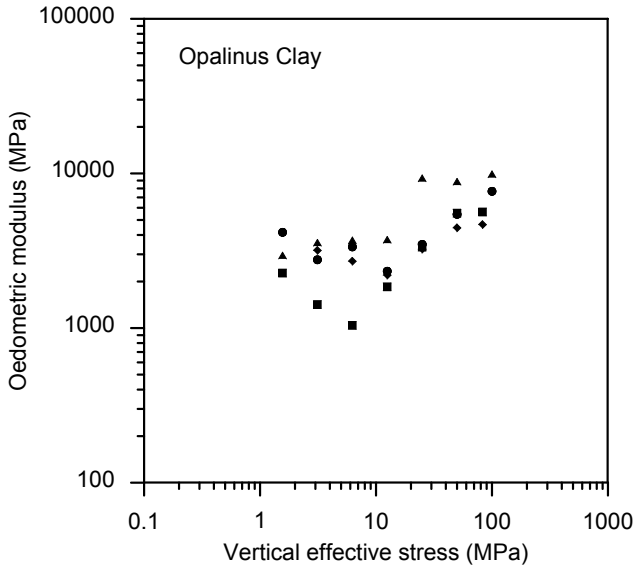

Fig. 3-34: Dependency of the Oedometric modulus on the vertical stress.

A further analysis can be performed comparing the results related to the elastic modulus of the material derived from the analysis of the triaxial tests with the elastic modulus derived from the high pressure oedometer tests for such S-samples.

During an oedometer test, where a condition of laterally constrained one-dimensional deformation is encounter, the radial stress acting on the sample is related to the vertical stress through the following relation which introduces the coefficient of earth pressure at rest k_0:

$$k_0 = \frac{\sigma'_h}{\sigma'_v}$$

The coefficient of earth pressure at rest k_0 is expressed as follows:

$k_0 = 1 - \sin\varphi'$ for normally consolidated conditions (Jaky 1948)

$k_0 = (1 - \sin\varphi') \left(\frac{\sigma'_p}{\sigma'_v}\right)^{\sin\varphi'}$ for overconsolidated conditions (Mayne & Kulhawy 1982)

where σ'_p is the vertical preconsolidation pressure evaluated from the oedometric tests and taken equal to 22 MPa in this analysis (see Ferrari et al. 2013), σ'_v is the vertical effective stress acting on the sample and φ' is the effective friction angle.

The oedometric modulus derived from the high pressure oedometric test is related to the elastic modulus of the material through the following relation[2] (Lambe and Whitman, 1979):

$$E = E_{oed} \frac{(1+v)(1-2v)}{(1-v)}$$

Thanks to the previous formulas it is possible to relate the elastic modulus as derived from the oedometric tests to the confining stress acting on the sample for different stress levels. Fig. 3-34 reports the oedometric moduli derived from the first loading and the NCL of different oedometric tests on Opalinus Clay (Ferrari et al. 2013); an average value of the E_{oed} is assumed for the increasing stress level and the corresponding elastic modulus is derived. In addition, the oedometric moduli derived from the unloading lines is also considered for the estimation of the elastic moduli as a function of the stress. The results are reported in Table 3-10.

[2] The relationship between the stresses and strains in the x and y directions can be expressed as $\varepsilon_x = \frac{1}{E}\left[\sigma'_x - \nu(\sigma'_z + \sigma'_y)\right]$ and $\varepsilon_y = \frac{1}{E}\left[\sigma'_y - \nu(\sigma'_z + \sigma'_x)\right]$. In oedometric condition $\sigma'_x = \sigma'_y$ and $\varepsilon_x = \varepsilon_y = 0$; setting these conditions in the previous equations the following relation is obtained: $\sigma'_x = \sigma'_z \frac{\nu}{1-\nu}$, which leads to $\varepsilon_z = \frac{1}{E}\left[\sigma'_z - 2\nu\sigma'_x\right] = \frac{\sigma'_z}{E}\left(1 - \frac{2\nu^2}{1-\nu}\right)$. The oedometric modulus is defined as the ratio of axial stress to axial strain in laterally confined compression, thus $E_{oed} = \frac{\sigma'_z}{\varepsilon_z} = E\frac{(1-\nu)}{(1+\nu)(1-2\nu)}$.

Tab. 3-10: Evaluation of the elastic modulus as a function of the confining stress from the high pressure oedometric tests.

First loading + NCL					Unloading lines			
σ'_v*	σ'_h	E_{oed}	E		σ'_v**	σ'_h	E_{oed}	E
[MPa]	[MPa]	[MPa]	[MPa]		[MPa]	[MPa]	[MPa]	[MPa]
5	4.7	3000	2863		6.2	6.1	2478	2365
10	8.1	4000	3818		6.2	6.1	3804	3631
30	17.3	6000	5727		25.0	14.4	8365	7983
60	34.6	8000	7635		82.7	47.7	6834	6523
100	57.7	10000	9544		82.7	47.7	10009	9553
					100.0	57.7	14237	13588

* Final value for the considered step

** Initial value for the considered step

Assumptions: $\varphi' = 25°$ as derived in the triaxial testing campain on S-samples
$\nu = 0.14$ as reported in Table 3-8.

The comparison of such results with those obtained from the analysis of the triaxial tests results are reported in Fig. 3-35 where the elastic modulus is represented as a function of the confining stress level.

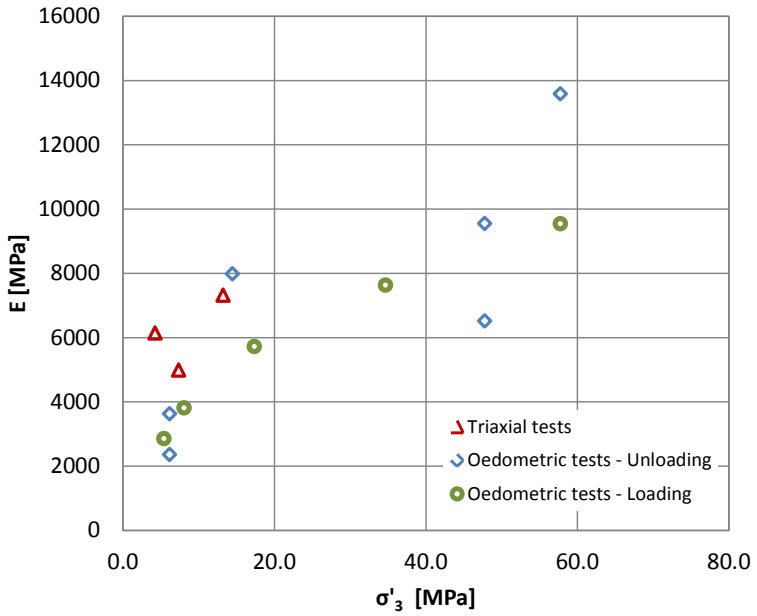

Fig. 3-35: Elastic modulus as a function of the confining effective stress obtained from the analysis of the triaxial tests and oedometric tests results.

4 Assessment of the relevance of coupled processes on the deformation behaviour

The assessment of the hydro-mechanical couplings is fundamental for the investigation of the behaviour of Opalinus Clay. The expressions obtained in the previous section related to the stiffness dependency on the confining pressure allow evaluating the stiffness that is expected for a confinement equal to zero, in the case of a saturated state of the material.

The same condition can be obtained in an UCS test since the lateral confinement of the material is equal to zero; on the other end, in this case unsaturated conditions are encountered since the samples are tested at the room relative humidity (saturation of the sample is not provided) thus, according to the psychrometric law it is reasonable to assume that certain suction is developed in the material. The comparison between the elastic moduli determined from the analysis of the UCS data and the elastic moduli derived from the expression in section 0 can highlight the effect of suction on the stiffness of the material.

The elastic modulus from the UCS tests (E_{UCS}) has been estimated on the loading-unloading loop thus ensuring an elastic response of the material. The values of the E_{UCS} and the elastic moduli derived from the previous expressions for a confining pressure equal to zero are reported in Fig. 4-1.

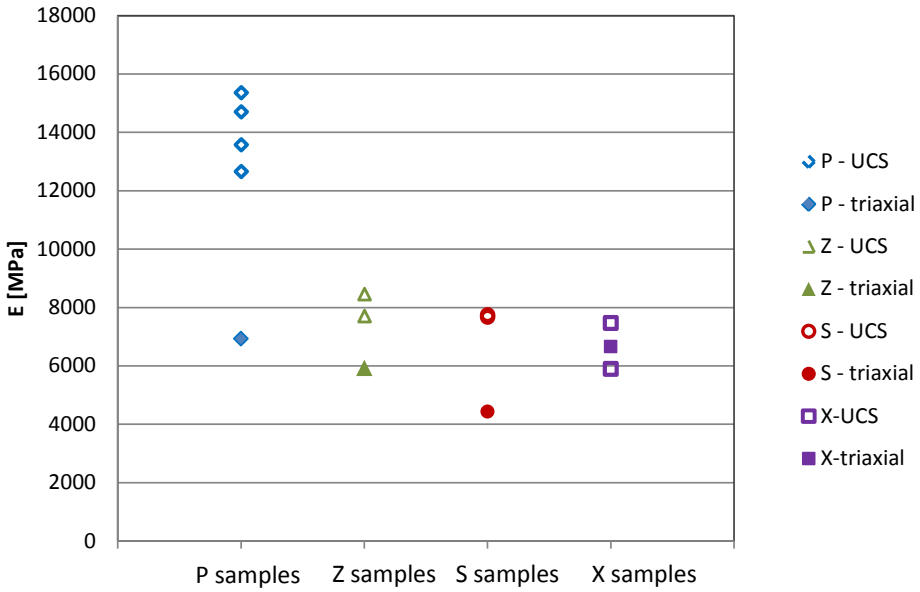

Fig. 4-1: Comparison of the elastic modulus derived from UCS and triaxial tests.

The increase in stiffness of the material due the presence of suction is observed. These findings are also confirmed by previous investigations conducted at LMS/EPFL on Opalinus Clay where the oedometric behaviour of the material has been tested at different suction values; the results are reported in Fig. 4-2 (Laloui et al. 2012), namely an increasing stiffness of the material with increasing suction.

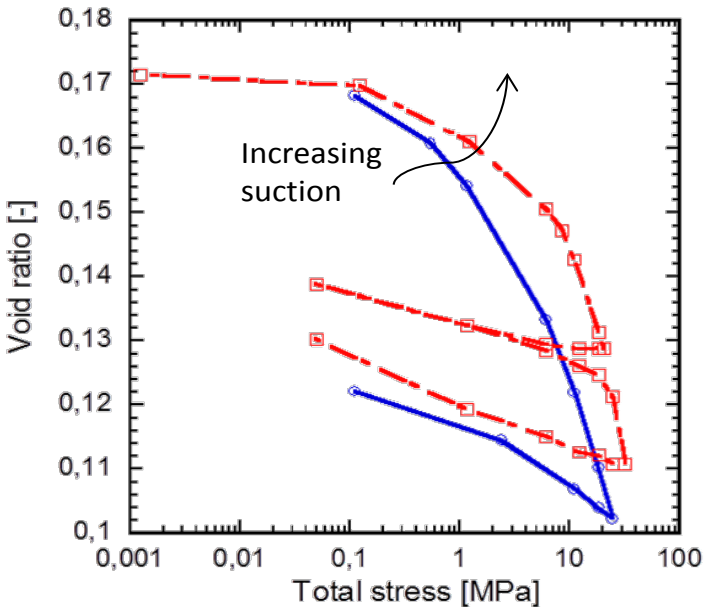

Fig. 4-2: Oedometric curves on Opalinus Clay at different suction values.

The deformation behaviour of Opalinus Clay is investigated in the light of available experimental results which show the porosity dependence on suction; the mentioned results have been obtained at LMS/EPFL and reported in Ferrari et al. (2013). The saturation of the material determines an important increase in porosity as shown in the free swelling tests in Fig. 4-3, while a decrease in the degree of saturation and thus the development of suction leads to a decrease in the porosity of the material as reported in Fig. 4-4.

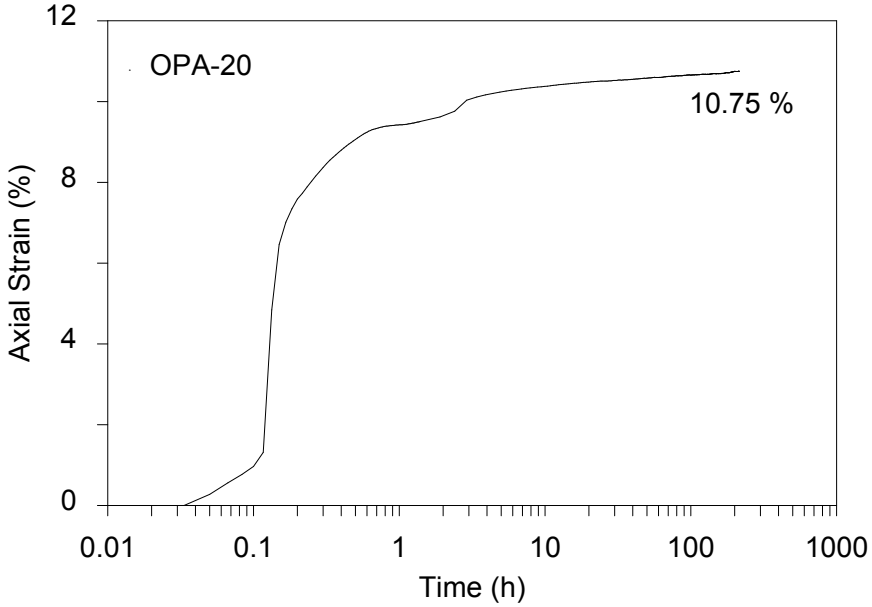

Fig. 4-3: Free swelling test on Opalinus Clay (Ferrari et al. 2013).

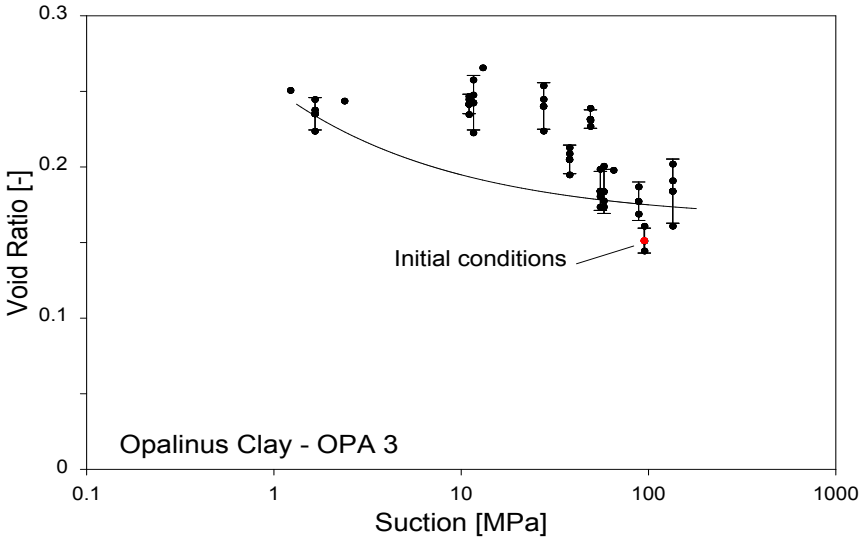

Fig. 4-4: Void ratio variation due to change in suction (Ferrari et al. 2013).

Changes in suction (or degree of saturation) increase the stiffness of the material, reduce its compressibility (Fig. 4-2) and determine changes in porosity. The analysis of the retention behaviour has highlighted the relation between the porosity variation with changes in suction (Fig. 4-4); however such analysis have been carried out under unstressed condition (Ferrari et al. 2013). As a consequence if the hydraulic loading is coupled with mechanical loading (i.e. changes in stress) the volumetric response of the material will be also affected. The coupled hydro-mechanical response of the material needs further investigation for a better understanding of such processes.

5 A generalised geomechanical framework for Opalinus Clay

The elaboration of a generalized geomechanical framework for Opalinus Clay requires the identification of the main features that characterize this formation. The objective of this chapter is to recall the main observations about the behaviour of Opalinus Clay highlighting the dependency of the material parameters. This is required to achieve a clear and complete view on the behaviour of the material thus allowing the determination of the main features that have to be considered in a constitutive modelling framework.

Anisotropy

The first aspect that characterises the behaviour of the Opalinus Clay formation is the marked anisotropy, thus the elasto-plastic parameters are different in relation to the loading orientation. The peak strength of the material is highly affected by the loading orientation: higher values of peak strength are observed for the loading orientation parallel to bedding while considerably lower peak strength values are observed for the orientation perpendicular to bedding. The lowest strength is found for the orientation of 45° respect to the bedding orientation. The elastic modulus of the material is considerably higher for the P-samples thus revealing a reduced compressibility in this sense; while lower values of elastic modulus are obtained for S and Z samples thus probably due to the presence (opening/closure) of the bedding.

Stress dependency

The confining stress influences the values of the elastic parameters; the increasing stiffness with the confining pressure is commonly observed together with the increasing strength of the material with the increasing stress level.

Post peak behaviour: brittle failure and softening

Interesting results are also observed in Corkum and Martin (2007) in relation to the Opalinus Clay shale in Mont Terri: first of all the increasing stiffness with confining pressure is observed: “The samples show brittle response at all confining stress levels. Surprisingly, no indication of a brittle-ductile transition was observed up to 20MPa (twice the estimated maximum past pressure)”.

Experimental evidence is available where the brittle failure and the softening of the material after the peak is observed even at slightly consolidated or normally consolidated conditions. The modelling of the behaviour of the material before the ultimate state conditions leads to the need to decouple the link between OC-NC conditions and softening-hardening behaviour. The softening after peak at slightly overconsolidated or normally consolidated conditions seems to be related to the disturbance of the material rather than to its overconsolidation state.

Further consideration on the constitutive modelling

In order to reproduce the behaviour of Opalinus Clay, a suitable constitutive model should take into account the observations reported in the previous paragraphs.

Nagra requested a brief statement on the suitability of the constitutive models in the code FLAC3D (©ITASCA) for simulating the deformation behavior of Opalinus Clay. FLAC3D offers a wide range of options of constitutive models among which the bilinear strain-hardening/softening ubiquitous joint model (ITASCA, 2009) was selected for Opalinus Clay. The model is able to take into account the presence of the bedding planes and it is based on a bilinear Mohr-Coulomb criterion with a tension cut off. However such model presents some limitations in the prediction of the response of Opalinus Clay which can be relevant depending on the stress paths involved in the problem to be analysed. The limitations can be summarized as follows:

- The elastic parameters considered in the model are not dependent on the confining stress, while such dependency is a main feature of the involved material.
- In such a bilinear model, the yielding due to an isotropic compression cannot be taken into account since no yield limit (cap) is encounter along an isotropic compression stress path; as a matter of fact, the hardening of the material is observed also when an isotropic stress increase is applied.
- In the Mohr-Coulomb model with a tension cut off, the cohesion, friction, dilation and tensile strength are constant while in the proposed bilinear strain-hardening/softening ubiquitous joint model the cohesion, friction, dilation and tensile strength may harden or soften after the development of plastic strains thus reproducing the hardening and softening of the material. However a change of strength parameters and thus a rotation and/or translation of the failure surface is not necessarily related to the hardening phenomena, this may not lead to a correct interpretation of the overall mechanical behaviour of the material.
- For a reliable interpretation of the Opalinus Clay behaviour the porosity variation needs to be assessed while this objective cannot be achieved when a model based on the Mohr-Coulomb failure criterion is used.
- Opalinus Clay is also characterized by a progressive plasticity which mobilizes before surpassing the yield limit; this means that the material can experience plastic deformations inside the external yield limit which translate in a progressive loss of stiffness induced by this activated plastic mechanism. Such feature cannot be taken into account in the majority of the constitutive models available thus resulting in an overestimation of the stiffness of the material.

6 Conclusions

This report presented a diagnostic analysis of the geomechanical data bases from the geothermal well Schlattingen SLA-1.

A wide range of geomechanical tests were taken into consideration in order to obtain a complete picture of the mechanical and hydro-mechanical response of the Opalinus Clay; the database taken into account for the analysis is specified in Chapter 2 together with the documents related to the detailed tests execution.

The diagnostic analysis of the geomechanical data base from the triaxial testing campaign includes considerations on the testing procedure, as well as an indepth analysis of the results from the triaxial testing campaign: the main diagnostic plots (p'-q, q–ε_a, ε_a–ε_v, Δu–ε_a) have been considered and the evaluation of the results in terms of the deformation mechanism of the material has been performed. The analysis of the saturation and consolidation procedures as well as the strain rate effect, allow for qualifying the individual tests. Accordingly, all tests were assessed in a traceable manner and a quality level between A and D was assigned to each test (Table 3-6). Subsequently the most reliable data were selected for determination of representative strength parameters (Table 3-7) and elastic properties of Opalinus Clay (Figs. 3-32 and 3-33).

The elastic properties of the material have been determined and further information has been gained thanks to the analysis of a series of UCS tests. The triaxial and UCS database together with a series of oedometric tests allowed gathering information about the dependency of the elastic modulus on the confining stress (Fig. 3-35) together with the understanding of the effect of suction on the elastic parameters of the material. Further considerations about the coupled hydro-mechanical behaviour of Opalinus Clay have been done taking into account the information provided by the results of a series of swelling tests and water retention curves (Figs. 4-3 and 4-4).

The diagnostic analysis allowed for identifying the main characteristics in the behaviour of Opalinus Clay, thus obtaining a complete view on the response of the material. Such features should be taken into account in a constitutive modelling framework development for Opalinus Clay. Further indications have been provided regarding the limitations of the constitutive models based on the Mohr-Coulomb failure criterion when adopted for the constitutive modelling of Opalinus Clay.

References

Al-Bazali T., Zhang J., Chenevert M.E., Sharma M.M. (2008): Experimental and numerical study on the impact of strain rate on failure characteristics of shales. Journal of Petroleum Science and Engineering 60, 194–204.

Albert, W., H.R. Bläsi, H. Madritsch, T. Vogt, H.P. Weber (2012): Geologie, Stratigraphie, Strukturgeologie, bohrlochgeophysikalisches Logging und Wasserproben der Geothermiebohrung Schlattingen SLA-1 (Rohdaten). Nagra Project Report NPB 12-16, Nagra, Wettingen, Switzerland.

Berge P.A. (1998): Pore Compressiblity in Rocks. Biot Conference on Poromechanics. Louvain-la-Neuve, Belgium. September 14-16.

Cook J. (1999): The Effects of Pore Pressure on the Mechanical and Physical Properties of Shales. *Oil & Gas Science and Technology – Rev. IFP,* Vol. 54, No. 6, pp. 695-701.

Corkum A.G., Martin C.D. (2007): The mechanical behaviour of weak mudstone (Opalinus Cly) at low stresses. International journal of rock mechanics & mining sciences 44, 196-209.

Ferrari A. and Laloui L. (2012): Advances in the testing of the hydro-mechanical behaviour of shales. In L. Laloui and A. Ferrari editors. Multiphysical Testing of Soils and Shales, pages 57-68, Springer.

Ferrari A., V. Favero, D. Manca and L. Laloui (2013): Geotechnical characterization of core samples from the geothermal well Schlattingen SLA-1 by LMS/EPFL. Nagra Work Report NAB 12-50, Nagra, Wettingen, Switzerland.

Hart D.J. (2000): Laboratory measurements of poroelastic constants and flow parameters and some associated phenomena. PhD Thesis, University of Wisconsis – Madison.

ITASCA (2009): FLAC3D (V. 4.0). Fast Lagrangian Analysis of Continua in 3 Dimensions. User's Guide.

Jahns, E. (2013): Geomechanical laboratory tests on Opalinus Clay cores from the bore hole Schlattingen SLA-1. Nagra Work Report NAB 13-18, Nagra, Wettingen, Switzerland.

Jaky J. (1948): Pressure in soils. 2nd ICSMFE, London, Vol. 1, pp 103-107.

Laloui L., A. Ferrari and S. Salager (2012): Testing the Thermo-Hydro-Mechanical Behaviour of a Shale. 3rd EAGE Shale Workshop, Barcelona.

Lambe, R. and V. Whitman (1979): Soil Mechanics. Wiley.

Mayne, P.W. and Kulhawy, F.H. (1982): K0-OCR relationships in soil. Journal of Geotechnical Engineering, Vol. 108 (GT6), 851-872.

Skempton A.W. (1954): The pore-pressure coefficients A and B. Géotechnique(4): 143-147.

Swan G., Cook J., Bruce S., Meehan, R. (1989): Strain Rate Effects in Kimmeridge Bay Shale. Int. J. Rock Mech. Min. Sci. & Geomech. Abstr. Vol. 26. No. 2. pp. 135-149.

Appendix A: Diagnostic plots of the geomechanical data bases from the SLA-1 borehole

S – Samples

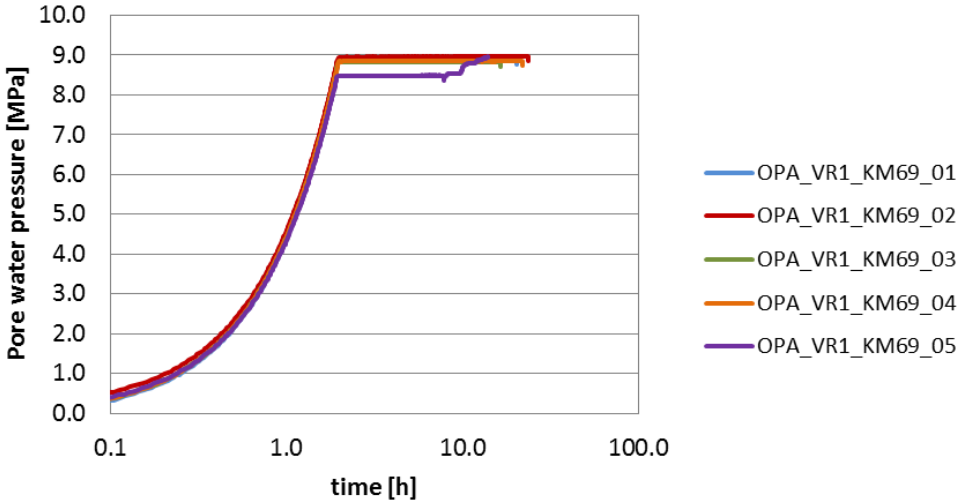

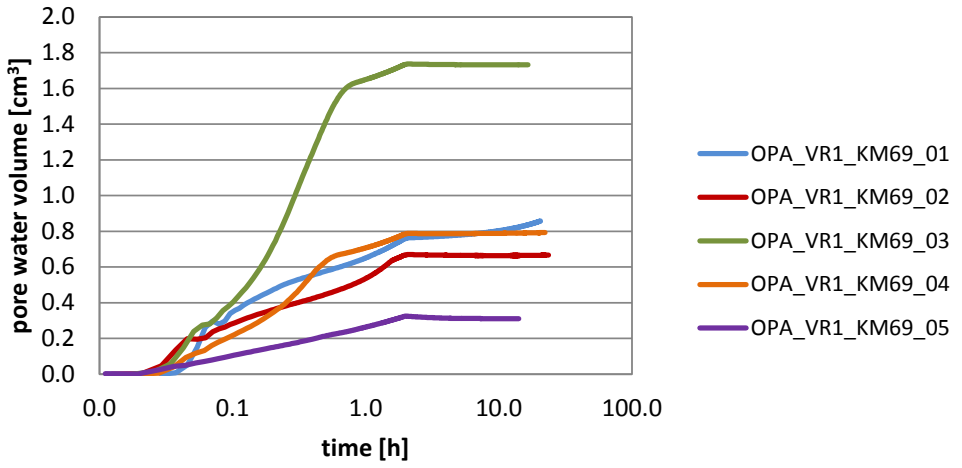

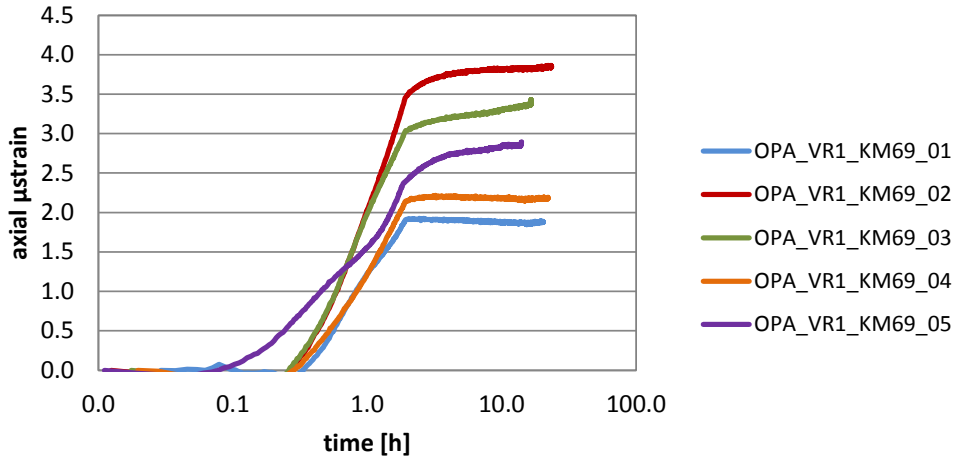
4.5
4.0
3.5
3.0
2.5
2.0
1.5
1.0
0.5
0.0
axial µstrain
0.0
0.1
1.0
10.0
100.0
time [h]
OPA_VR1_KM69_01
OPA_VR1_KM69_02
OPA_VR1_KM69_03
OPA_VR1_KM69_04
OPA_VR1_KM69_05

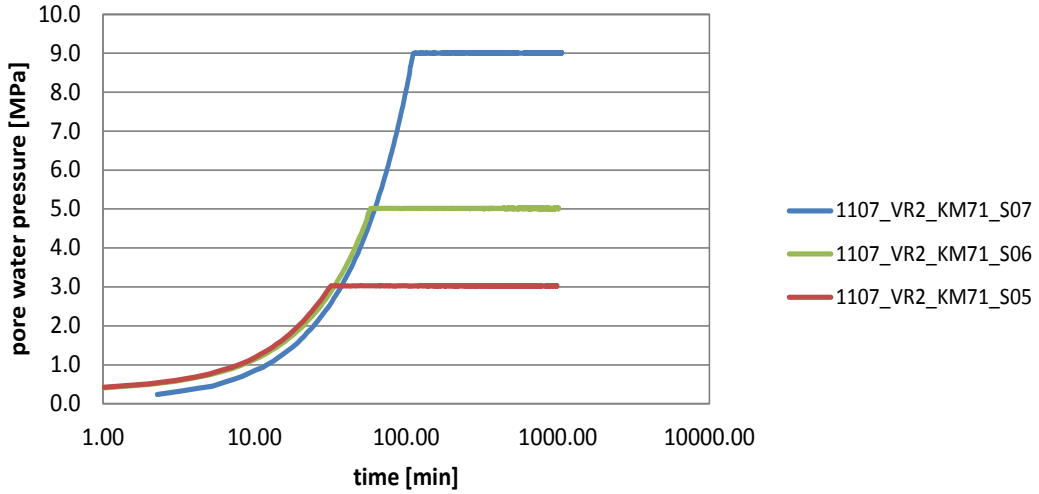
10.0
9.0
8.0
7.0
6.0
5.0
4.0
3.0
2.0
1.0
0.0
pore water pressure [MPa]
1.00
10.00
100.00
1000.00
10000.00
time [min]
1107_VR2_KM71_S07
1107_VR2_KM71_S06
1107_VR2_KM71_S05

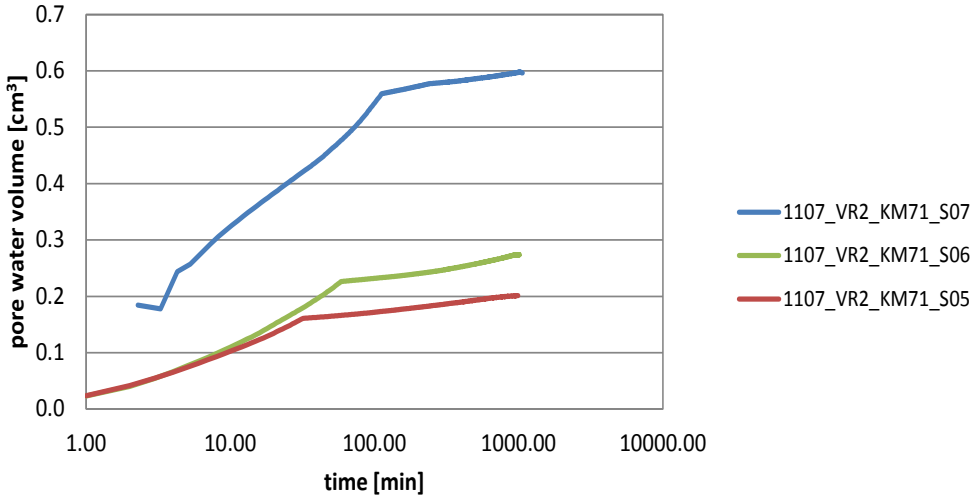
0.7
0.6
0.5
0.4
0.3
0.2
0.1
0.0
pore water volume [cm³]
1.00
10.00
100.00
1000.00
10000.00
time [min]
1107_VR2_KM71_S07
1107_VR2_KM71_S06
1107_VR2_KM71_S05

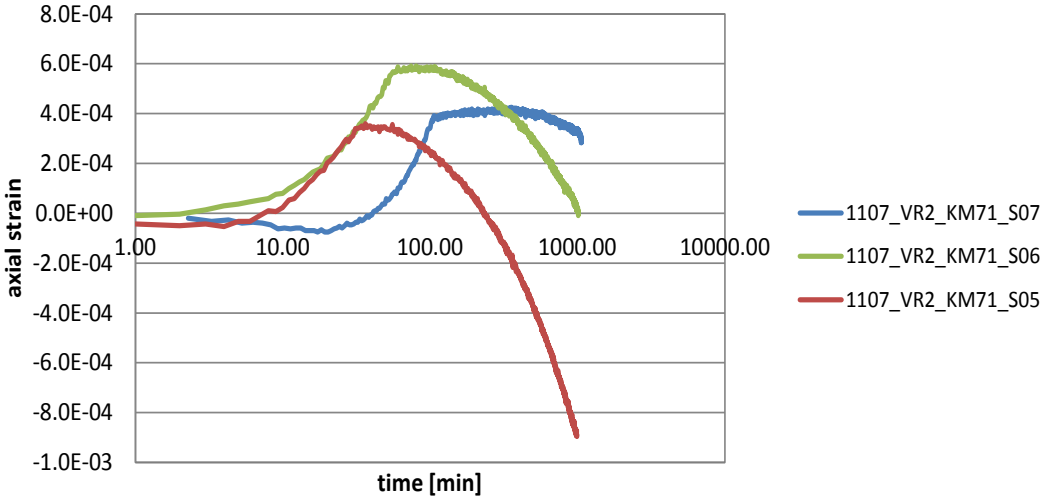
8.0E-04
6.0E-04
4.0E-04
2.0E-04
0.0E+00
-2.0E-04
-4.0E-04
-6.0E-04
-8.0E-04
-1.0E-03
axial strain
1.00
10.00
100.00
1000.00
10000.00
time [min]
1107_VR2_KM71_S07
1107_VR2_KM71_S06
1107_VR2_KM71_S05

P – Samples

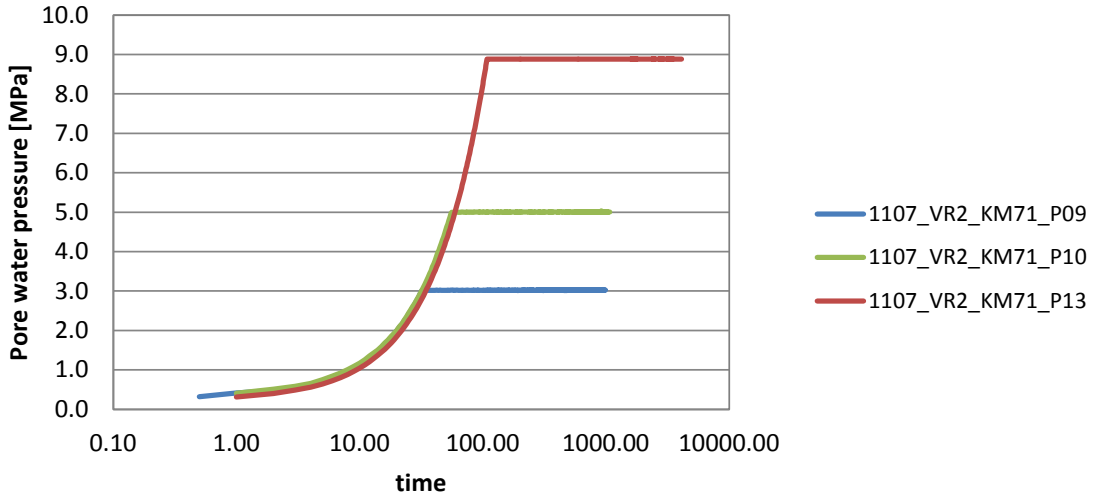
10.0
9.0
8.0
7.0
6.0
5.0
4.0
3.0
2.0
1.0
0.0
Pore water pressure [MPa]
0.10
1.00
10.00
100.00
1000.00
10000.00
time
1107_VR2_KM71_P09
1107_VR2_KM71_P10
1107_VR2_KM71_P13

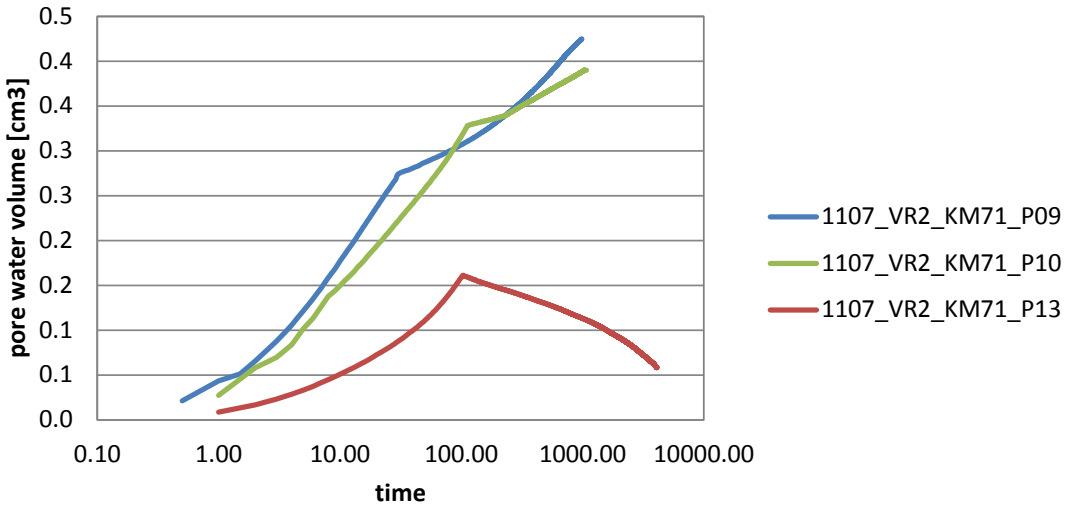
0.5
0.4
0.4
0.3
0.3
0.2
0.2
0.1
0.1
0.0
pore water volume [cm3]
0.10
1.00
10.00
100.00
1000.00
10000.00
time
1107_VR2_KM71_P09
1107_VR2_KM71_P10
1107_VR2_KM71_P13

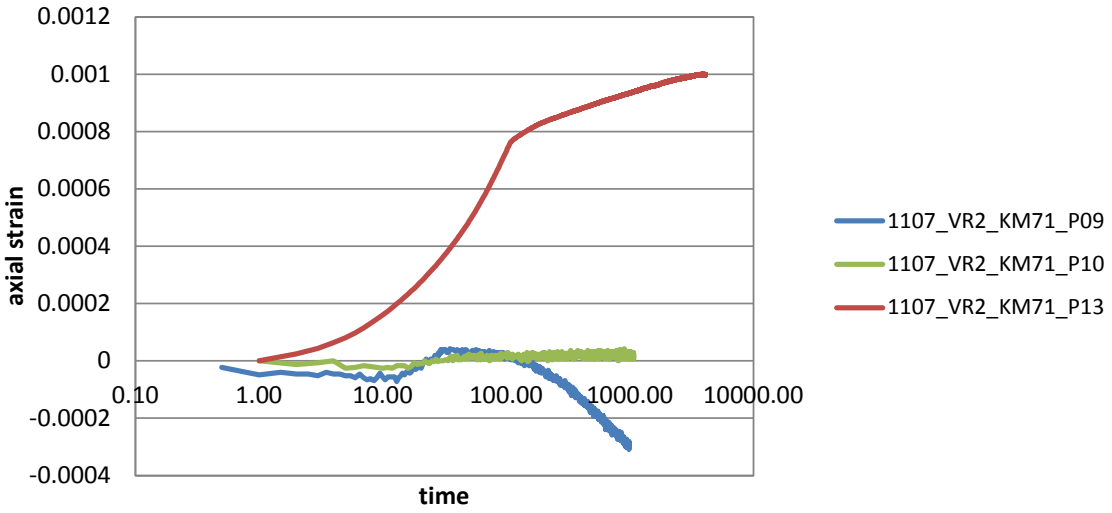
0.0012
0.001
0.0008
0.0006
0.0004
0.0002
0
-0.0002
-0.0004
axial strain
0.10
1.00
10.00
100.00
1000.00
10000.00
time
1107_VR2_KM71_P09
1107_VR2_KM71_P10
1107_VR2_KM71_P13

X – Samples

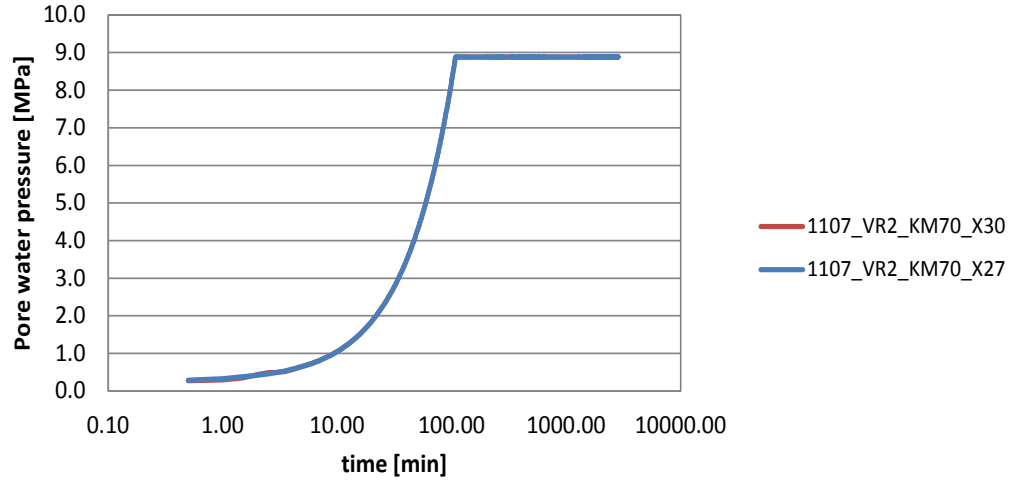
Pore water pressure [MPa]
10.0
9.0
8.0
7.0
6.0
5.0
4.0
3.0
2.0
1.0
0.0
0.10
1.00
10.00
100.00
1000.00
10000.00
time [min]
1107_VR2_KM70_X30
1107_VR2_KM70_X27

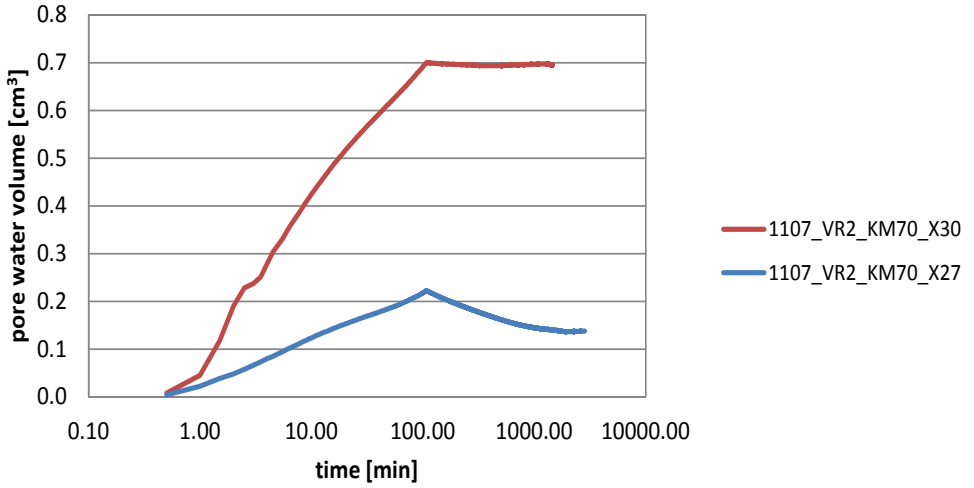
pore water volume [cm³]
0.8
0.7
0.6
0.5
0.4
0.3
0.2
0.1
0.0
0.10
1.00
10.00
100.00
1000.00
10000.00
time [min]
1107_VR2_KM70_X30
1107_VR2_KM70_X27

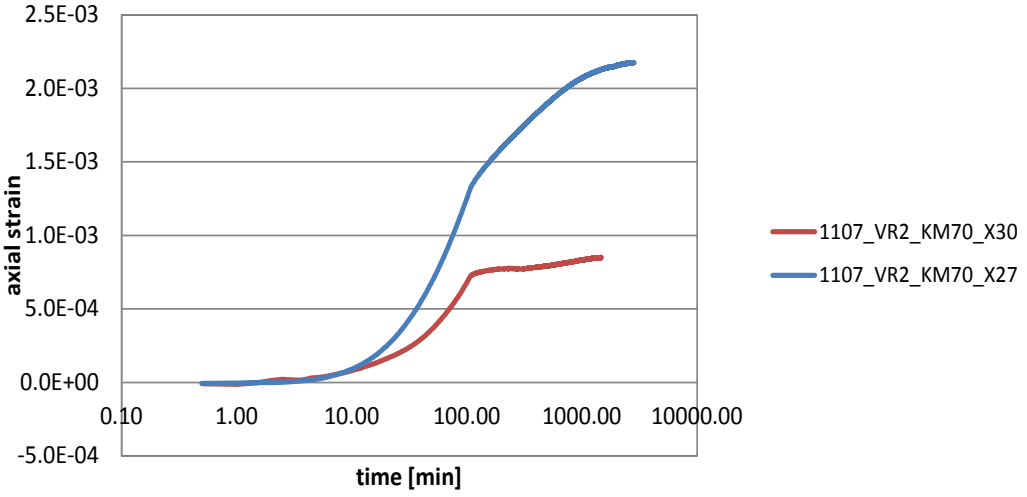
axial strain
2.5E-03
2.0E-03
1.5E-03
1.0E-03
5.0E-04
0.0E+00
-5.0E-04
0.10
1.00
10.00
100.00
1000.00
10000.00
time [min]
1107_VR2_KM70_X30
1107_VR2_KM70_X27

Z – Samples

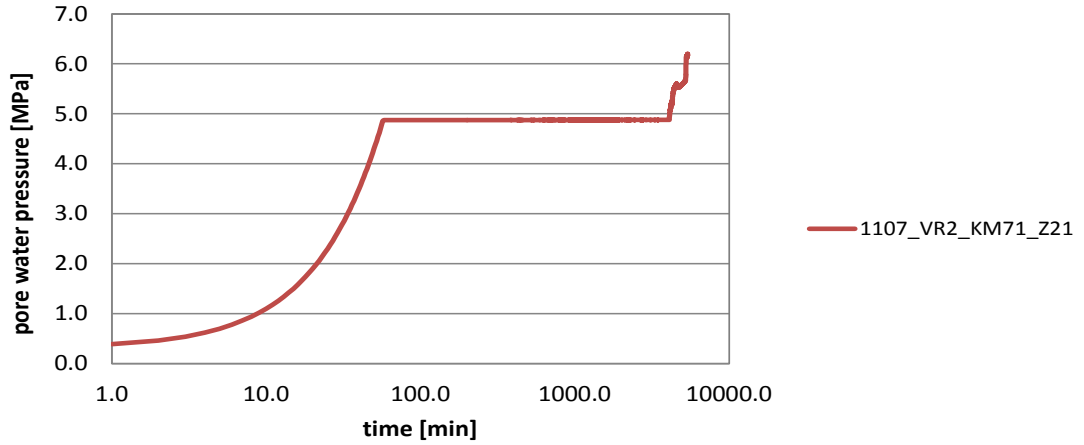
7.0
6.0
5.0
4.0
3.0
2.0
1.0
0.0
pore water pressure [MPa]
1.0
10.0
100.0
1000.0
10000.0
time [min]
1107_VR2_KM71_Z21

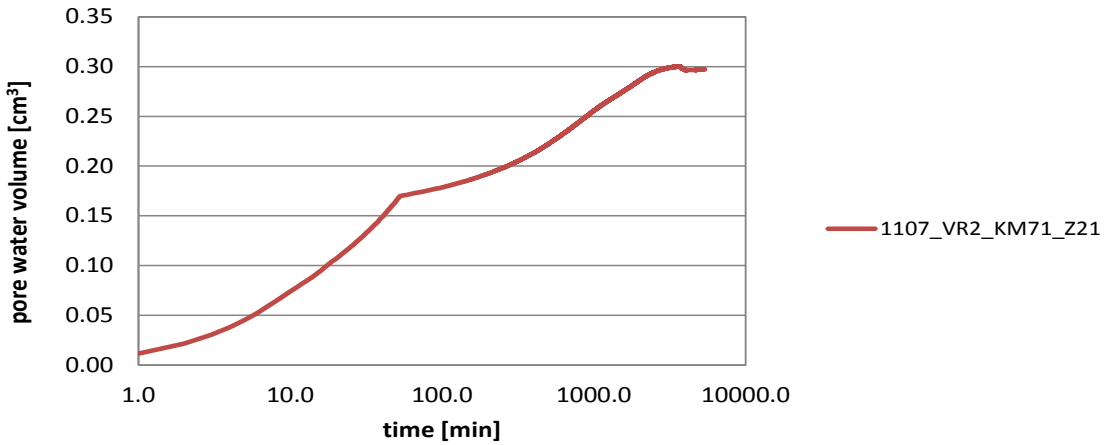
0.35
0.30
0.25
0.20
0.15
0.10
0.05
0.00
pore water volume [cm³]
1.0
10.0
100.0
1000.0
10000.0
time [min]
1107_VR2_KM71_Z21

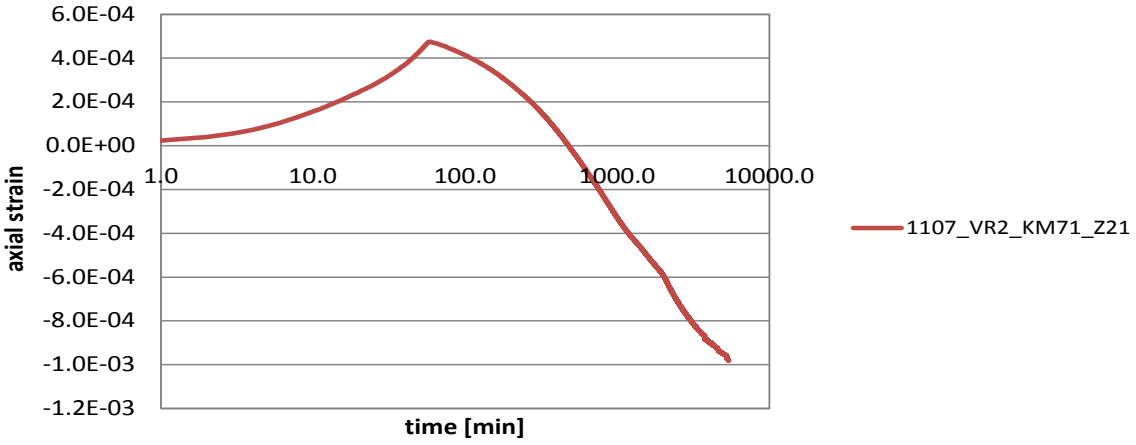
6.0E-04
4.0E-04
2.0E-04
0.0E+00
-2.0E-04
-4.0E-04
-6.0E-04
-8.0E-04
-1.0E-03
-1.2E-03
axial strain
1.0
10.0
100.0
1000.0
10000.0
time [min]
1107_VR2_KM71_Z21

Triaxial tests - Diagnostic Plots

S – Samples

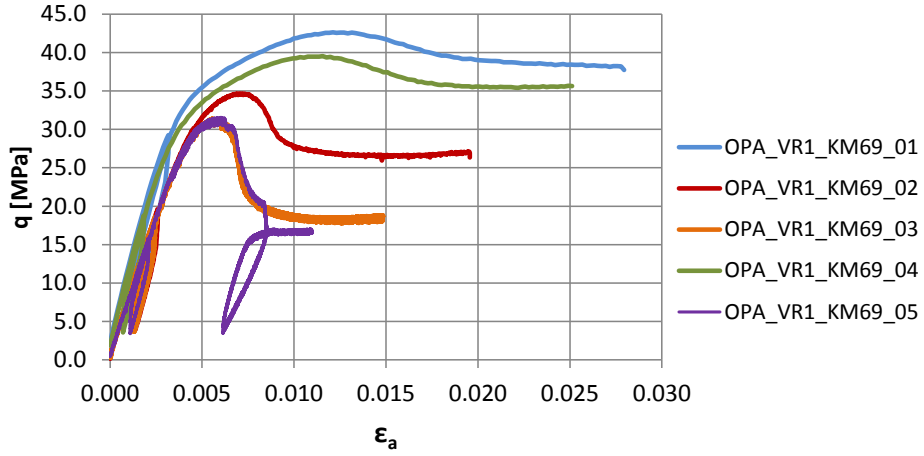

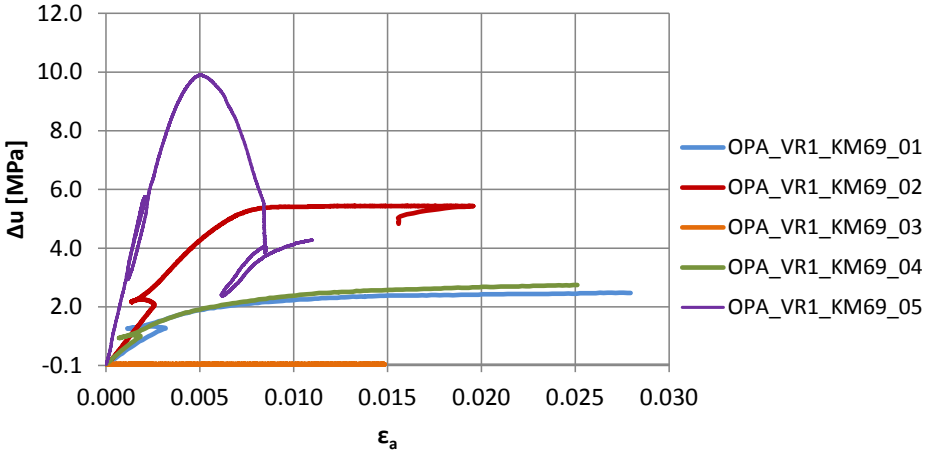

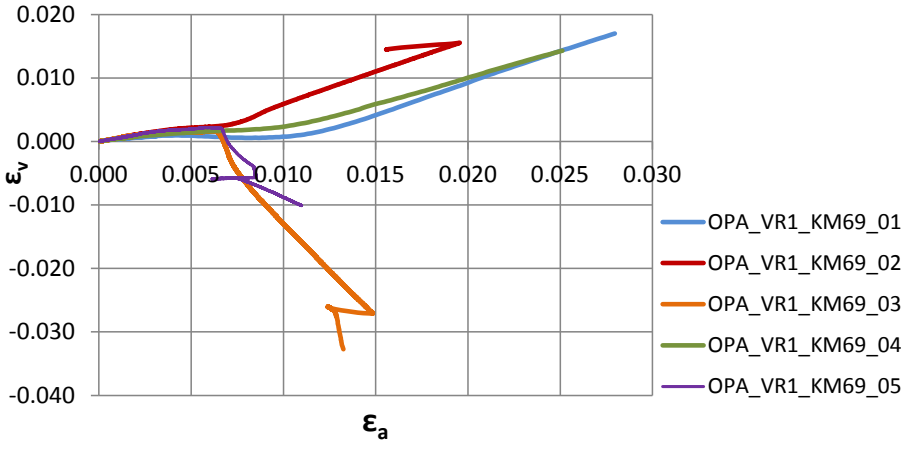

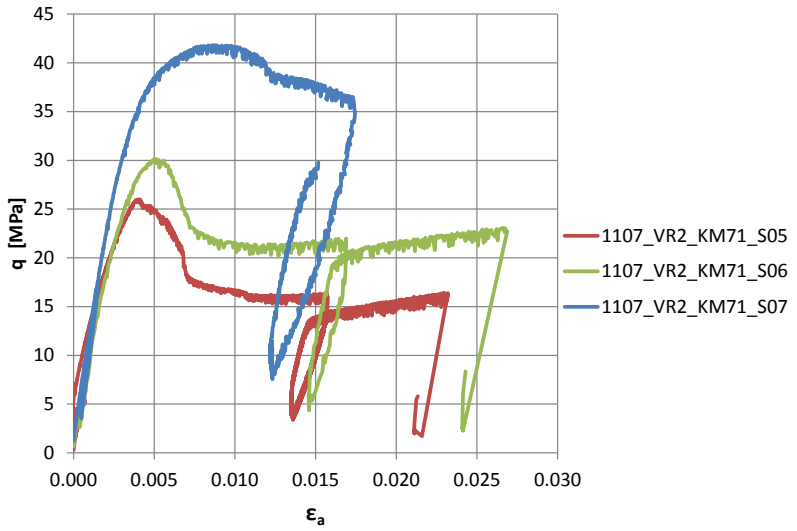
45
40
35
30
25
20
15
10
5
0
q [MPa]
0.000
0.005
0.010
0.015
0.020
0.025
0.030
εa
1107_VR2_KM71_S05
1107_VR2_KM71_S06
1107_VR2_KM71_S07

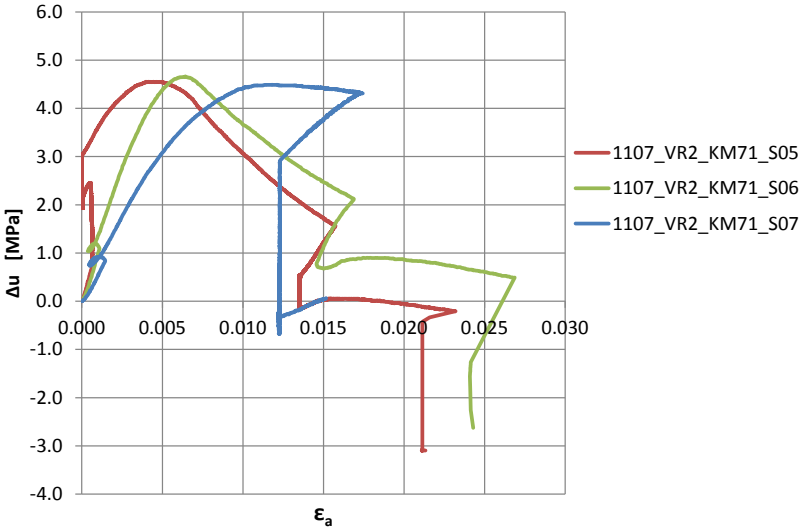
6.0
5.0
4.0
3.0
2.0
1.0
0.0
-1.0
-2.0
-3.0
-4.0
Δu [MPa]
0.000
0.005
0.010
0.015
0.020
0.025
0.030
εa
1107_VR2_KM71_S05
1107_VR2_KM71_S06
1107_VR2_KM71_S07

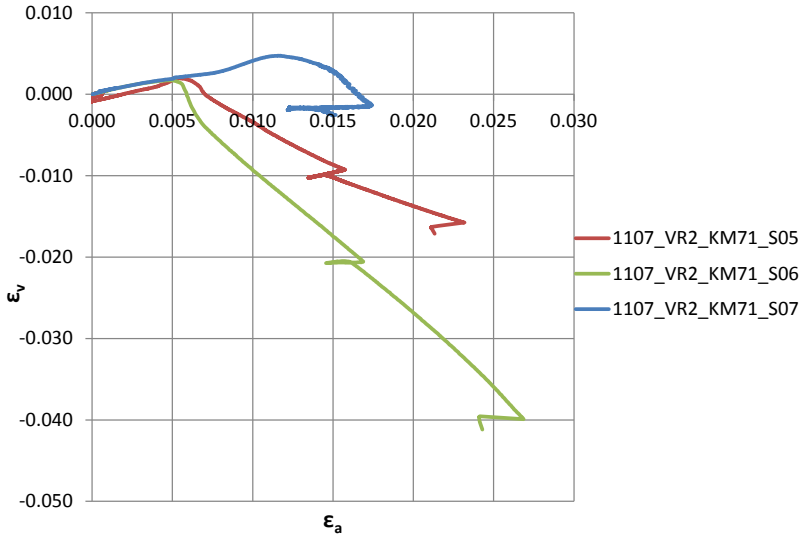
0.010
0.000
-0.010
-0.020
-0.030
-0.040
-0.050
εv
0.000
0.005
0.010
0.015
0.020
0.025
0.030
εa
1107_VR2_KM71_S05
1107_VR2_KM71_S06
1107_VR2_KM71_S07

P – Samples

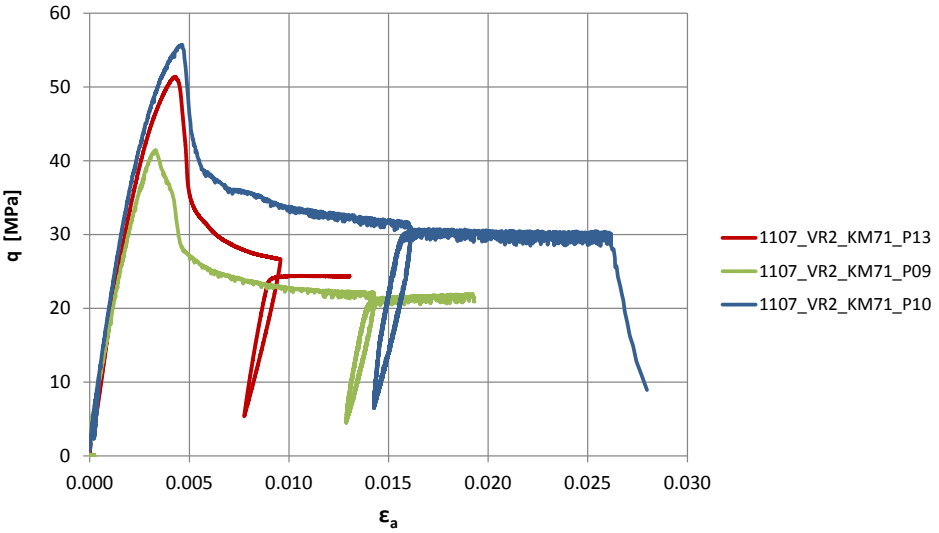
60
50
40
30
20
10
0
q [MPa]
0.000
0.005
0.010
0.015
0.020
0.025
0.030
εa
1107_VR2_KM71_P13
1107_VR2_KM71_P09
1107_VR2_KM71_P10

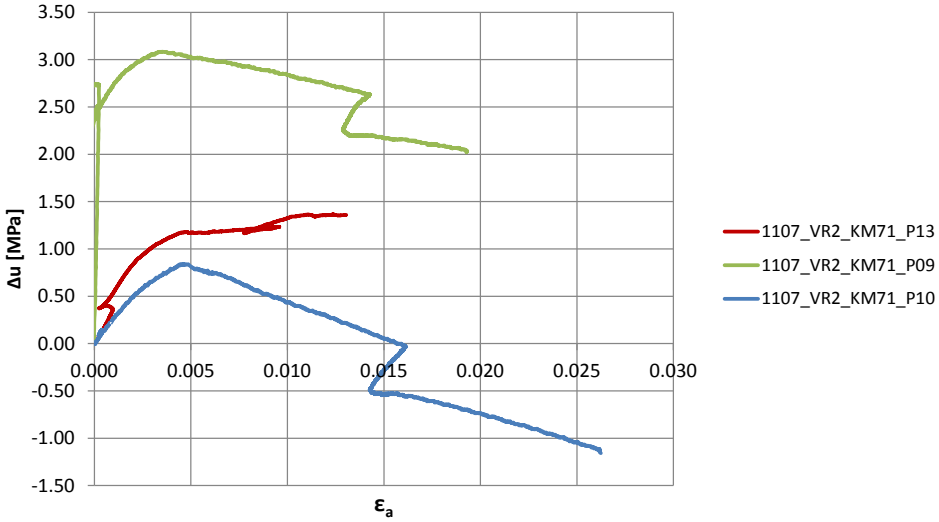
3.50
3.00
2.50
2.00
1.50
1.00
0.50
0.00
-0.50
-1.00
-1.50
Δu [MPa]
0.000
0.005
0.010
0.015
0.020
0.025
0.030
εa
1107_VR2_KM71_P13
1107_VR2_KM71_P09
1107_VR2_KM71_P10

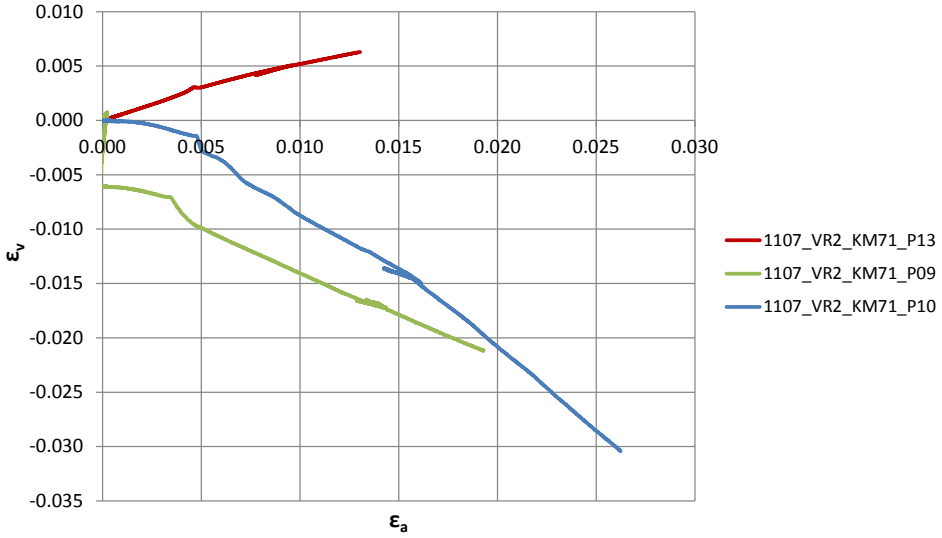
0.010
0.005
0.000
-0.005
-0.010
-0.015
-0.020
-0.025
-0.030
-0.035
0.000
0.005
0.010
0.015
0.020
0.025
0.030
εv
εa
1107_VR2_KM71_P13
1107_VR2_KM71_P09
1107_VR2_KM71_P10

X – Samples

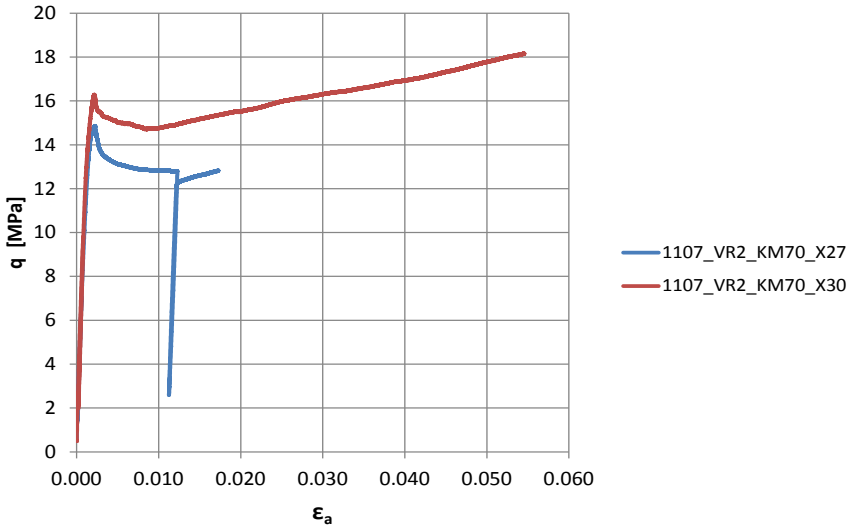
20
18
16
14
12
10
8
6
4
2
0
q [MPa]
0.000
0.010
0.020
0.030
0.040
0.050
0.060
εa
1107_VR2_KM70_X27
1107_VR2_KM70_X30

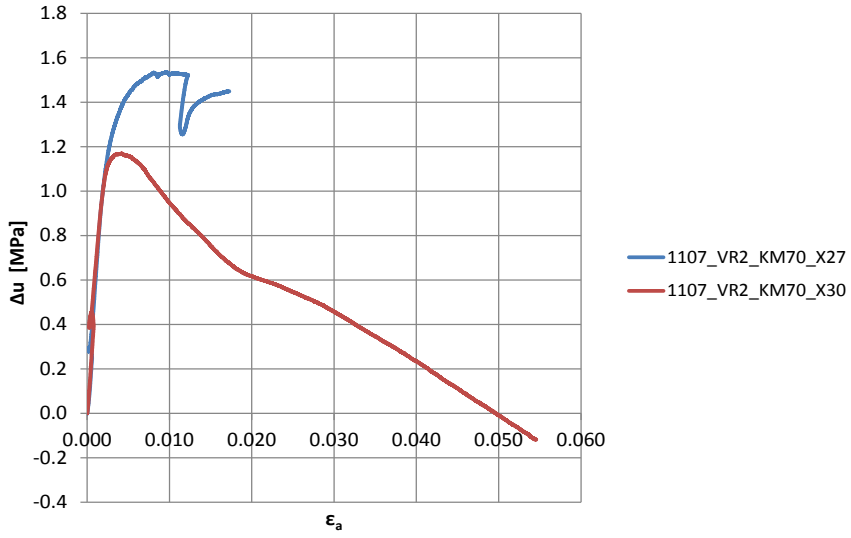
1.8
1.6
1.4
1.2
1.0
0.8
0.6
0.4
0.2
0.0
-0.2
-0.4
Δu [MPa]
0.000
0.010
0.020
0.030
0.040
0.050
0.060
εa
1107_VR2_KM70_X27
1107_VR2_KM70_X30

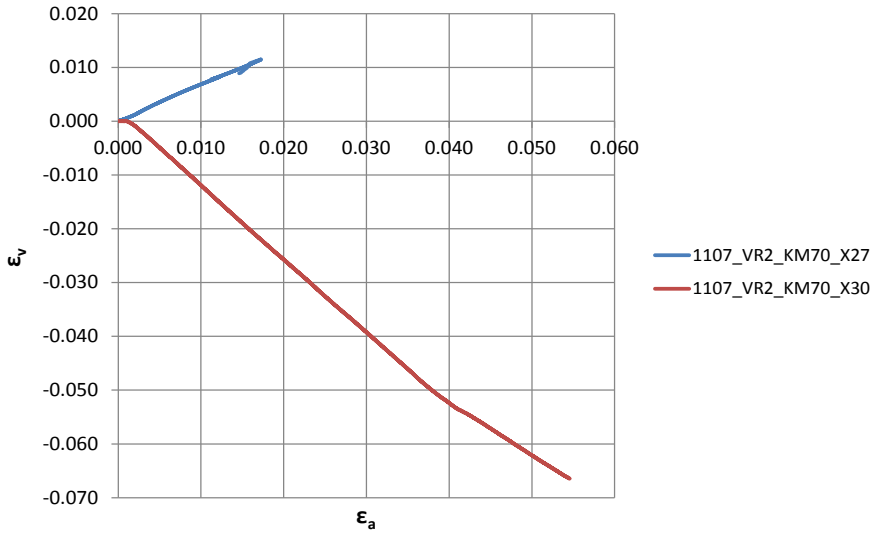
0.020
0.010
0.000
-0.010
-0.020
-0.030
-0.040
-0.050
-0.060
-0.070
0.000
0.010
0.020
0.030
0.040
0.050
0.060
εv
εa
1107_VR2_KM70_X27
1107_VR2_KM70_X30

UCS TESTS

S – Samples

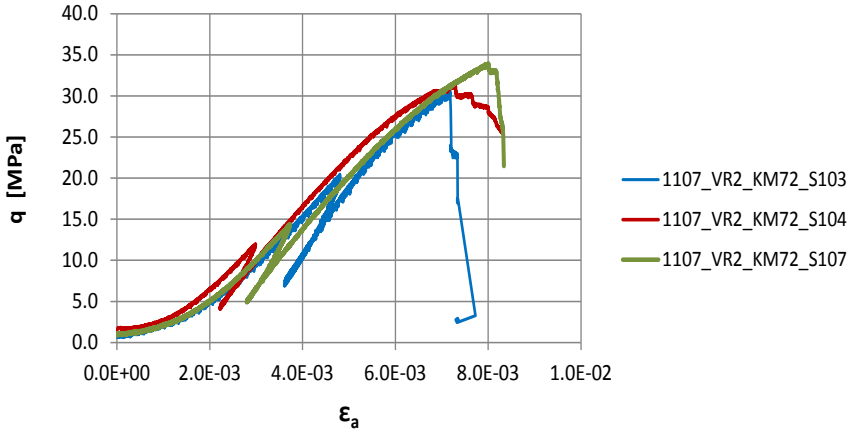

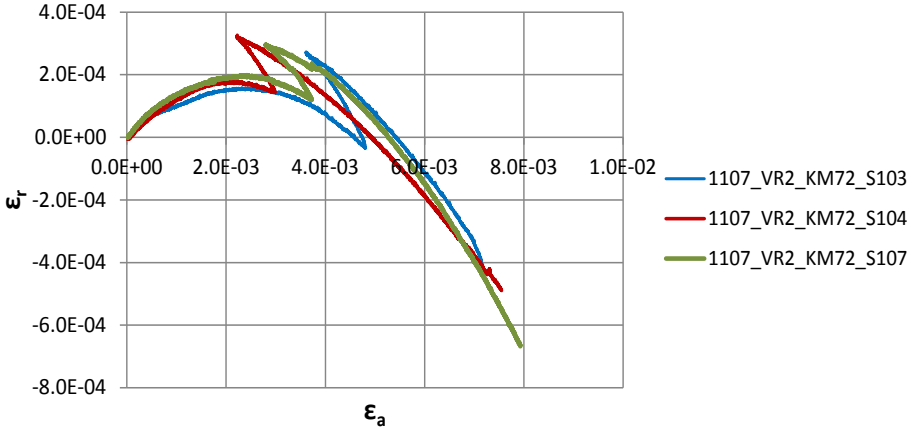

P - Samples

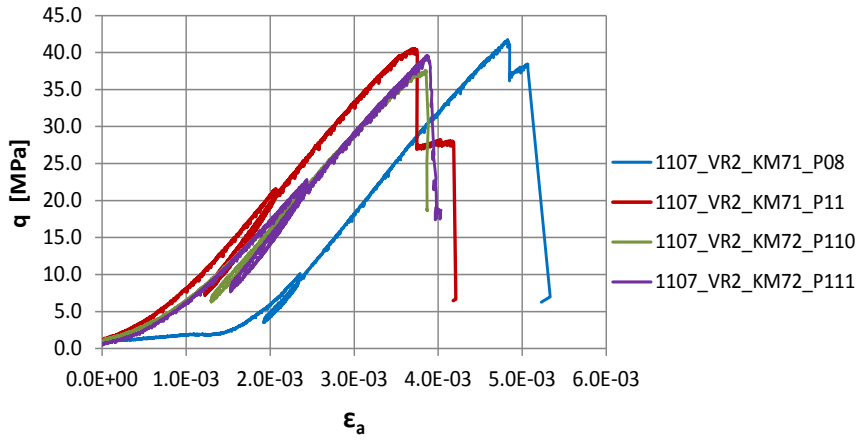
45.0
40.0
35.0
30.0
25.0
20.0
15.0
10.0
5.0
0.0
q [MPa]
0.0E+00 1.0E-03 2.0E-03 3.0E-03 4.0E-03 5.0E-03 6.0E-03
εa
1107_VR2_KM71_P08
1107_VR2_KM71_P11
1107_VR2_KM72_P110
1107_VR2_KM72_P111

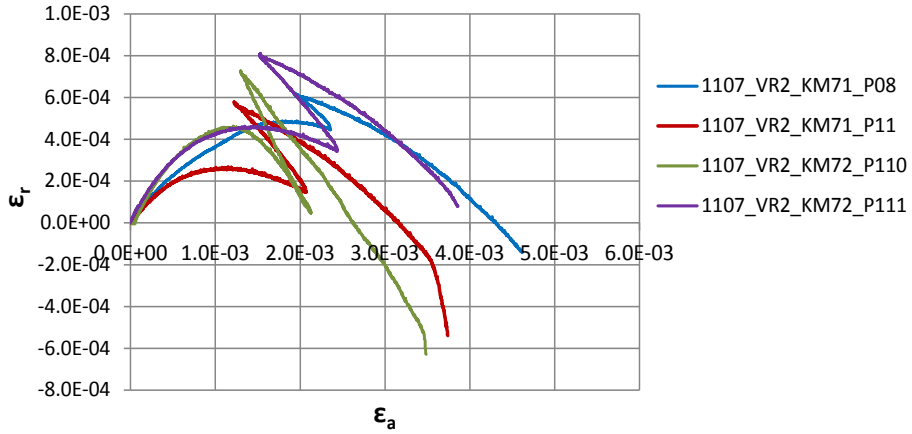
1.0E-03
8.0E-04
6.0E-04
4.0E-04
2.0E-04
0.0E+00
-2.0E-04
-4.0E-04
-6.0E-04
-8.0E-04
εr
0.0E+00 1.0E-03 2.0E-03 3.0E-03 4.0E-03 5.0E-03 6.0E-03
εa
1107_VR2_KM71_P08
1107_VR2_KM71_P11
1107_VR2_KM72_P110
1107_VR2_KM72_P111

X – Samples

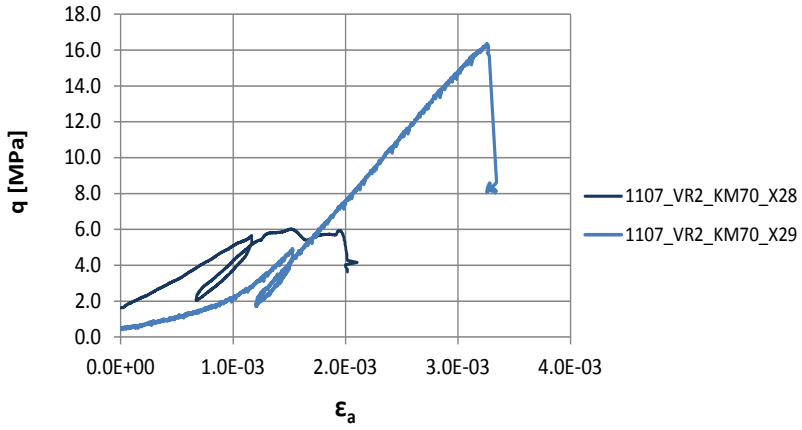
18.0
16.0
14.0
12.0
10.0
8.0
6.0
4.0
2.0
0.0
q [MPa]
0.0E+00
1.0E-03
2.0E-03
3.0E-03
4.0E-03
εa
1107_VR2_KM70_X28
1107_VR2_KM70_X29

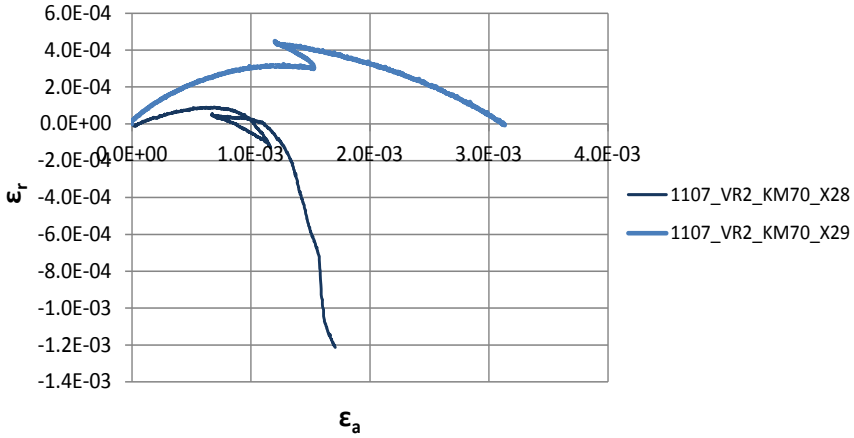
6.0E-04
4.0E-04
2.0E-04
0.0E+00
-2.0E-04
-4.0E-04
-6.0E-04
-8.0E-04
-1.0E-03
-1.2E-03
-1.4E-03
εr
0.0E+00
1.0E-03
2.0E-03
3.0E-03
4.0E-03
εa
1107_VR2_KM70_X28
1107_VR2_KM70_X29

Z – Samples

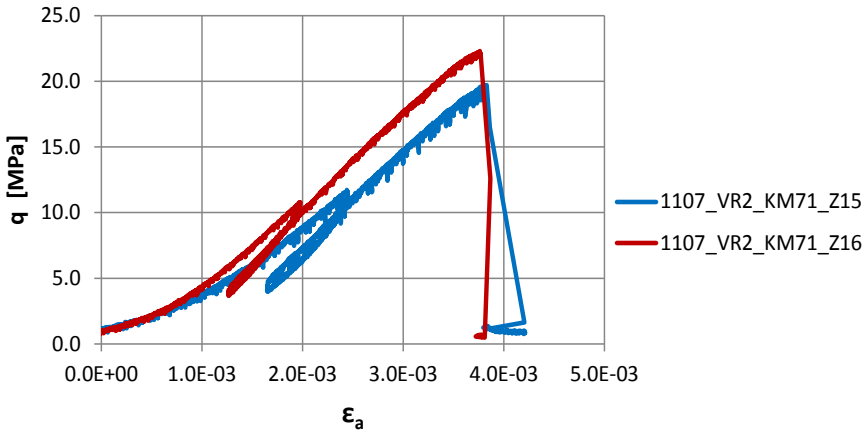
25.0
20.0
15.0
10.0
5.0
0.0
q [MPa]
0.0E+00
1.0E-03
2.0E-03
3.0E-03
4.0E-03
5.0E-03
εa
1107_VR2_KM71_Z15
1107_VR2_KM71_Z16

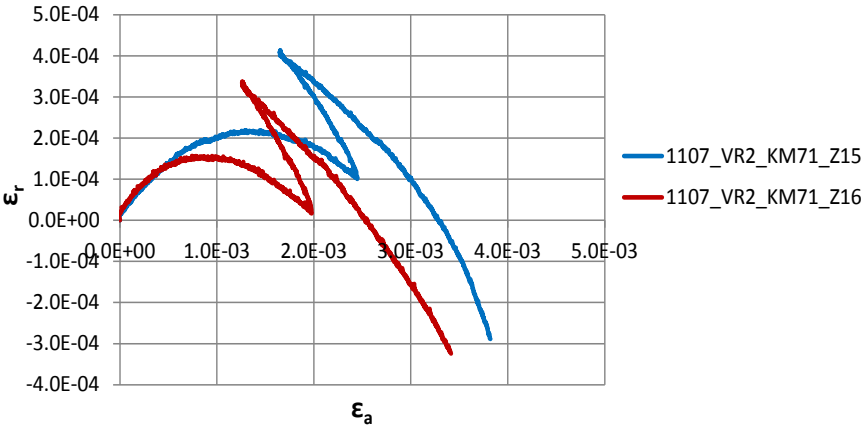
5.0E-04
4.0E-04
3.0E-04
2.0E-04
1.0E-04
0.0E+00
-1.0E-04
-2.0E-04
-3.0E-04
-4.0E-04
εr
0.0E+00
1.0E-03
2.0E-03
3.0E-03
4.0E-03
5.0E-03
εa
1107_VR2_KM71_Z15
1107_VR2_KM71_Z16

Appendix B: Structure of the electronic data base

Overview

Auxiliary digital files containing the whole set of data were made available to NAGRA. The electronic data base ensures the traceability of the reported raw data and the results of data analyses and collects all graphical data representations. The electronic data base is organized in the 2 main directories:

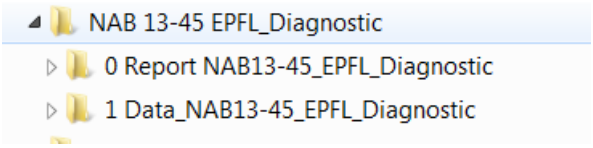

The detailed description of the contents of the directory "1 Data NAB13-45_EPFL-Diagnostic"

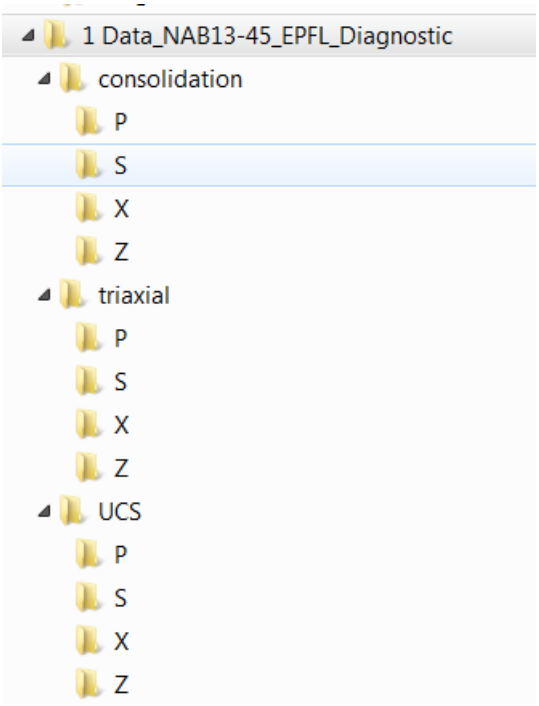

The data sub-directory "consolidation"

The data sub-directory contains all data analyses on P, S, X and Z samples. The sub-directory "P" comprises the EXCEL Files:

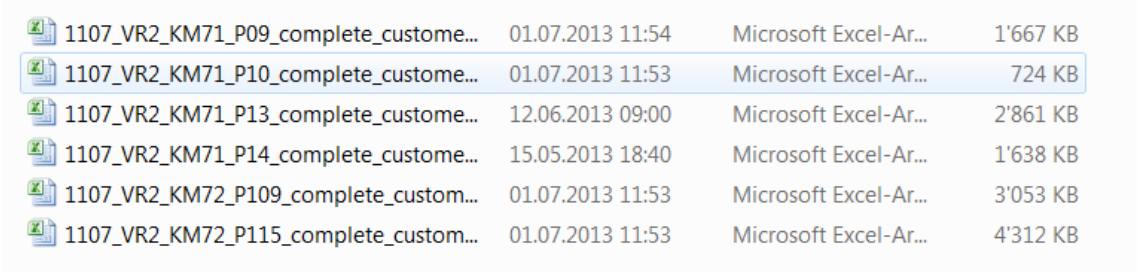

The sub-directory "S" comprises the EXCEL Files:

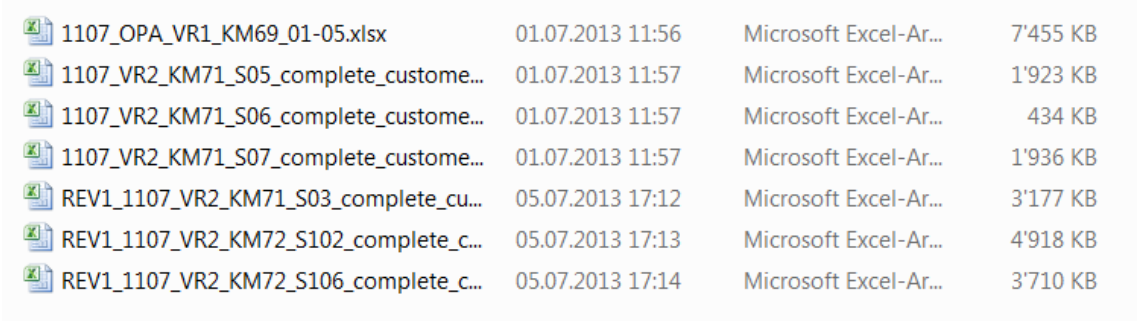

1107_OPA_VR1_KM69_01-05.xlsx	01.07.2013 11:56	Microsoft Excel-Ar...	7'455 KB
1107_VR2_KM71_S05_complete_custome...	01.07.2013 11:57	Microsoft Excel-Ar...	1'923 KB
1107_VR2_KM71_S06_complete_custome...	01.07.2013 11:57	Microsoft Excel-Ar...	434 KB
1107_VR2_KM71_S07_complete_custome...	01.07.2013 11:57	Microsoft Excel-Ar...	1'936 KB
REV1_1107_VR2_KM71_S03_complete_cu...	05.07.2013 17:12	Microsoft Excel-Ar...	3'177 KB
REV1_1107_VR2_KM72_S102_complete_c...	05.07.2013 17:13	Microsoft Excel-Ar...	4'918 KB
REV1_1107_VR2_KM72_S106_complete_c...	05.07.2013 17:14	Microsoft Excel-Ar...	3'710 KB

The sub-directory “X" comprises the EXCEL Files:

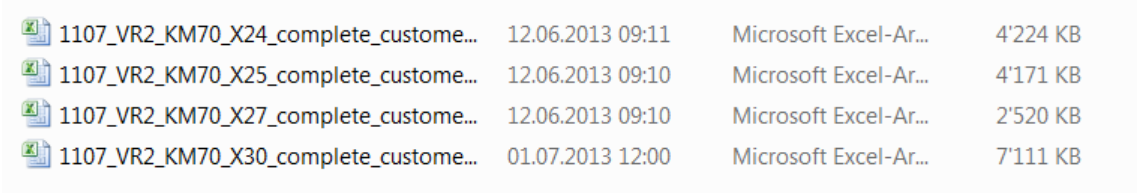

1107_VR2_KM70_X24_complete_custome...	12.06.2013 09:11	Microsoft Excel-Ar...	4'224 KB
1107_VR2_KM70_X25_complete_custome...	12.06.2013 09:10	Microsoft Excel-Ar...	4'171 KB
1107_VR2_KM70_X27_complete_custome...	12.06.2013 09:10	Microsoft Excel-Ar...	2'520 KB
1107_VR2_KM70_X30_complete_custome...	01.07.2013 12:00	Microsoft Excel-Ar...	7'111 KB

The sub-directory "Z" comprises the EXCEL Files:

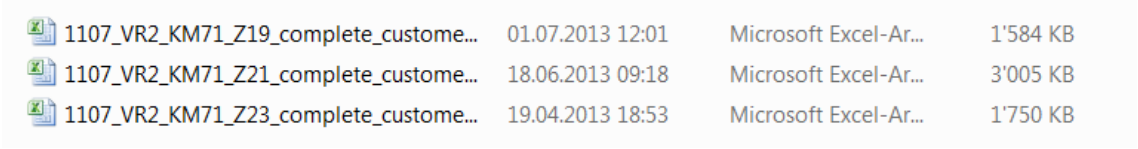

1107_VR2_KM71_Z19_complete_custome...	01.07.2013 12:01	Microsoft Excel-Ar...	1'584 KB
1107_VR2_KM71_Z21_complete_custome...	18.06.2013 09:18	Microsoft Excel-Ar...	3'005 KB
1107_VR2_KM71_Z23_complete_custome...	19.04.2013 18:53	Microsoft Excel-Ar...	1'750 KB

The data sub-directory "triaxial"

The data sub-directory contains all data analyses on P, S, X and Z samples. The sub-directory "P" comprises the EXCEL Files:

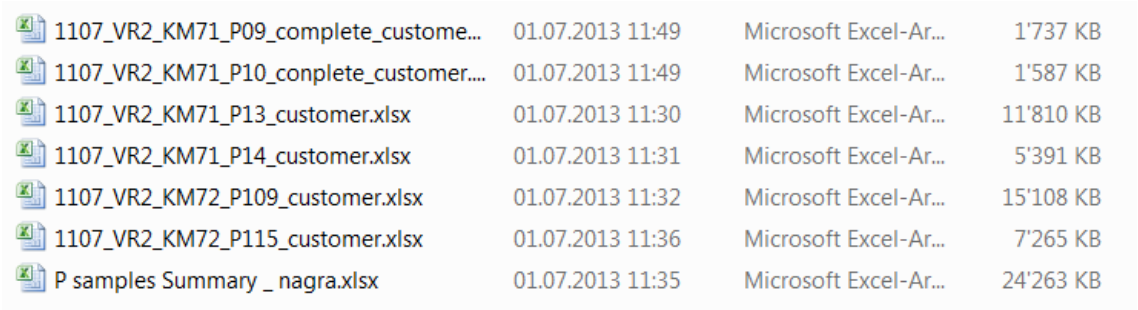

1107_VR2_KM71_P09_complete_custome...	01.07.2013 11:49	Microsoft Excel-Ar...	1'737 KB
1107_VR2_KM71_P10_conplete_customer....	01.07.2013 11:49	Microsoft Excel-Ar...	1'587 KB
1107_VR2_KM71_P13_customer.xlsx	01.07.2013 11:30	Microsoft Excel-Ar...	11'810 KB
1107_VR2_KM71_P14_customer.xlsx	01.07.2013 11:31	Microsoft Excel-Ar...	5'391 KB
1107_VR2_KM72_P109_customer.xlsx	01.07.2013 11:32	Microsoft Excel-Ar...	15'108 KB
1107_VR2_KM72_P115_customer.xlsx	01.07.2013 11:36	Microsoft Excel-Ar...	7'265 KB
P samples Summary _ nagra.xlsx	01.07.2013 11:35	Microsoft Excel-Ar...	24'263 KB

The sub-directory "S" comprises the EXCEL Files:

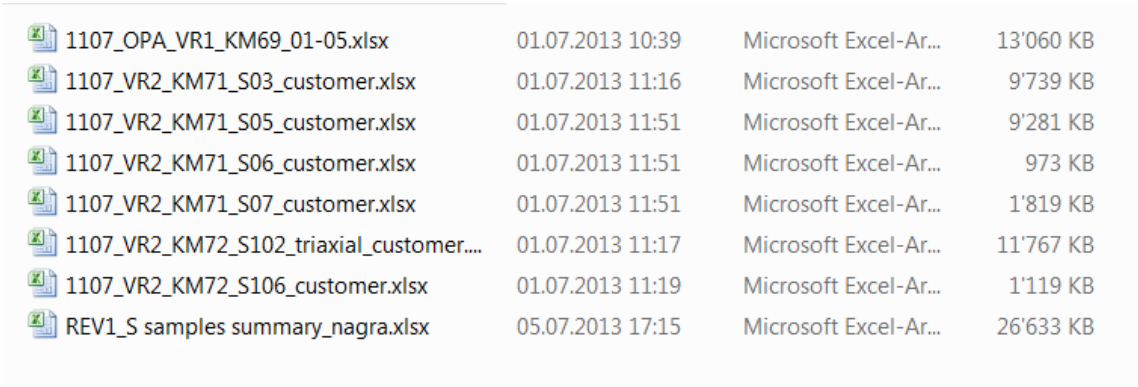

1107_OPA_VR1_KM69_01-05.xlsx	01.07.2013 10:39	Microsoft Excel-Ar...	13'060 KB
1107_VR2_KM71_S03_customer.xlsx	01.07.2013 11:16	Microsoft Excel-Ar...	9'739 KB
1107_VR2_KM71_S05_customer.xlsx	01.07.2013 11:51	Microsoft Excel-Ar...	9'281 KB
1107_VR2_KM71_S06_customer.xlsx	01.07.2013 11:51	Microsoft Excel-Ar...	973 KB
1107_VR2_KM71_S07_customer.xlsx	01.07.2013 11:51	Microsoft Excel-Ar...	1'819 KB
1107_VR2_KM72_S102_triaxial_customer....	01.07.2013 11:17	Microsoft Excel-Ar...	11'767 KB
1107_VR2_KM72_S106_customer.xlsx	01.07.2013 11:19	Microsoft Excel-Ar...	1'119 KB
REV1_S samples summary_nagra.xlsx	05.07.2013 17:15	Microsoft Excel-Ar...	26'633 KB

The sub-directory “X" comprises the EXCEL Files:

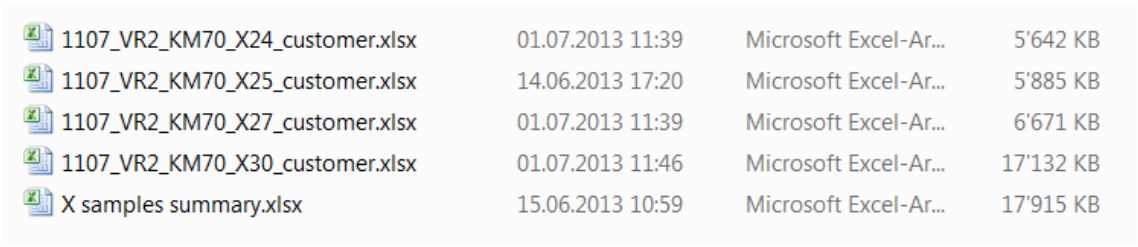

1107_VR2_KM70_X24_customer.xlsx	01.07.2013 11:39	Microsoft Excel-Ar...	5'642 KB
1107_VR2_KM70_X25_customer.xlsx	14.06.2013 17:20	Microsoft Excel-Ar...	5'885 KB
1107_VR2_KM70_X27_customer.xlsx	01.07.2013 11:39	Microsoft Excel-Ar...	6'671 KB
1107_VR2_KM70_X30_customer.xlsx	01.07.2013 11:46	Microsoft Excel-Ar...	17'132 KB
X samples summary.xlsx	15.06.2013 10:59	Microsoft Excel-Ar...	17'915 KB

The sub-directory "Z" comprises the EXCEL Files:

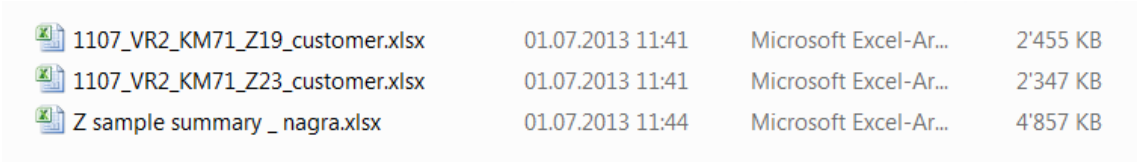

1107_VR2_KM71_Z19_customer.xlsx	01.07.2013 11:41	Microsoft Excel-Ar...	2'455 KB
1107_VR2_KM71_Z23_customer.xlsx	01.07.2013 11:41	Microsoft Excel-Ar...	2'347 KB
Z sample summary _ nagra.xlsx	01.07.2013 11:44	Microsoft Excel-Ar...	4'857 KB

The data sub-directory "UCS"

The data sub-directory contains all data analyses on P, S, X and Z samples. The sub-directory "P" comprises the EXCEL Files:

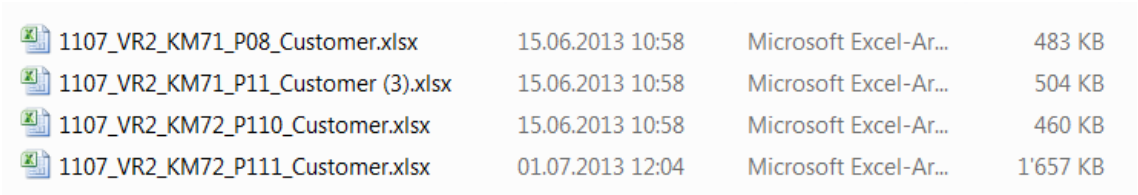

1107_VR2_KM71_P08_Customer.xlsx	15.06.2013 10:58	Microsoft Excel-Ar...	483 KB
1107_VR2_KM71_P11_Customer (3).xlsx	15.06.2013 10:58	Microsoft Excel-Ar...	504 KB
1107_VR2_KM72_P110_Customer.xlsx	15.06.2013 10:58	Microsoft Excel-Ar...	460 KB
1107_VR2_KM72_P111_Customer.xlsx	01.07.2013 12:04	Microsoft Excel-Ar...	1'657 KB

The sub-directory "S" comprises the EXCEL Files:

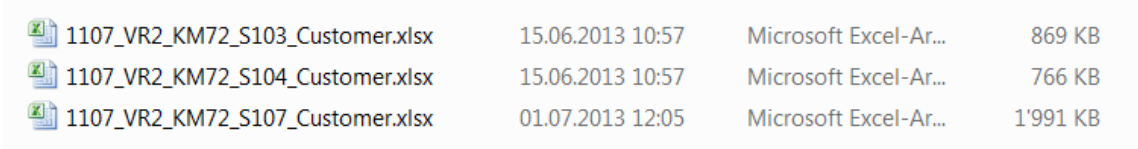

1107_VR2_KM72_S103_Customer.xlsx	15.06.2013 10:57	Microsoft Excel-Ar...	869 KB
1107_VR2_KM72_S104_Customer.xlsx	15.06.2013 10:57	Microsoft Excel-Ar...	766 KB
1107_VR2_KM72_S107_Customer.xlsx	01.07.2013 12:05	Microsoft Excel-Ar...	1'991 KB

The sub-directory “X" comprises the EXCEL Files:

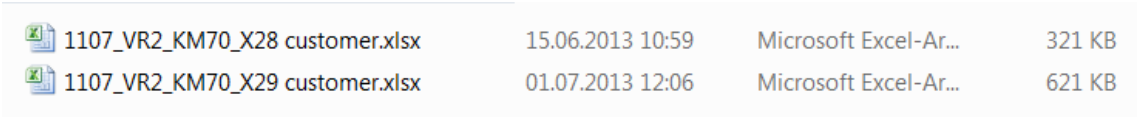

The sub-directory "Z" comprises the EXCEL Files: